

This discussion paper is/has been under review for the journal *Climate of the Past* (CP). Please refer to the corresponding final paper in CP if available.

Effects of CO₂, continental distribution, topography and vegetation changes on the climate at the Middle Miocene: a model study

A.-J. Henrot¹, L. François², E. Favre², M. Butzin³, M. Ouberdous², and G. Munhoven¹

¹Laboratory of Atmospheric and Planetary Physics, University of Liège, Liège, Belgium

²Unité de Modélisation du Climat et des Cycles Biogéochimiques, University of Liège, Liège, Belgium

³MARUM – Center for Marine Environmental Sciences, University of Bremen, Bremen, Germany

Received: 16 March 2010 – Accepted: 6 April 2010 – Published: 14 April 2010

Correspondence to: A.-J. Henrot (alexandra.henrot@ulg.ac.be)

Published by Copernicus Publications on behalf of the European Geosciences Union.

Middle Miocene climate modelling experiments

A.-J. Henrot et al.

Title Page

Abstract

Introduction

Conclusions

References

Tables

Figures

◀

▶

◀

▶

Back

Close

Full Screen / Esc

Printer-friendly Version

Interactive Discussion



Abstract

The Middle Miocene was one of the last warm periods of the Neogene, culminating with the Middle Miocene Climatic Optimum (MMCO, approximately 17–15 Ma). Several proxy-based reconstructions support warmer and more humid climate during the MMCO. The mechanisms responsible for the warming at MMCO and particularly the role of the atmospheric carbon dioxide CO₂ are still highly debated. Here we carried out a series of sensitivity experiments with the model of intermediate complexity Planet Simulator, investigating the contributions of the absence of ice on the continents, the opening of the Central American and Eastern Tethys Seaways, the lowering of the topography on land, the effect of various atmospheric CO₂ concentrations and the vegetation retroaction.

Our results show that a higher than present-day CO₂ concentration is necessary to generate a warmer climate at all latitudes at the Middle Miocene, in agreement with the terrestrial proxy reconstructions which suggest high atmospheric CO₂ concentrations at MMCO. Nevertheless, the changes in sea-surface conditions and the lowering of the topography on land also produce significant local warming that may, locally, even be stronger than the CO₂ induced temperature increases. The lowering of the topography leads to a more zonal atmospheric circulation and allows the westerly flow to continue over the lowered Plateaus at mid-latitudes. The reduced height of the Tibetan Plateau notably prevents the development of a monsoon-like circulation, whereas the reduction of elevations of the North American and European reliefs strongly increases precipitation from northwestern to eastern Europe. The changes in vegetation cover contributes to maintain and even to intensify the the warm and humid conditions produced by the other factors, suggesting that the vegetation-climate interactions could help to improve the model-data comparison.

CPD

6, 489–535, 2010

Middle Miocene climate modelling experiments

A.-J. Henrot et al.

Title Page

Abstract

Introduction

Conclusions

References

Tables

Figures



Back

Close

Full Screen / Esc

Printer-friendly Version

Interactive Discussion



1 Introduction

In a long-term climatic cooling trend, the Middle Miocene represents one of the last warm periods of the Neogene, culminating with the Middle Miocene Climatic Optimum, MMCO, that occurred at approximately 17–15 Ma (Zachos et al., 2001). Various proxy data support warmer and more humid climate during the MMCO (Zachos et al., 2001; Mosbrugger et al., 2005; Bruch et al., 2007). Proxy-based studies suggest a warming at mid-latitudes of about +6 °C (Flower and Kennett, 1994) and a weak equator-to-pole latitudinal temperature gradient (Bruch et al., 2007). However, the climate mechanisms responsible for the warming at MMCO and, in particular, the role of the atmospheric carbon dioxide CO₂, are still highly debated. Frequently, elevated greenhouse gas concentrations are cited as primary contributors to past warm climates (Shellito et al., 2003). However, estimates for the concentration of CO₂ in the atmosphere at MMCO range from levels that are typical for Pleistocene glaciations to nearly twice the modern value. Pagani et al. (1999) calculated CO₂ levels of 180 to 290 ppmv from marine $\delta^{13}\text{C}$ biological isotopic fractionation. Marine pH reconstructions from $\delta^{11}\text{B}$ also suggest a low CO₂ level between 140 and 300 ppmv (Pearson and Palmer, 2000), supporting a decoupling between CO₂ and temperature during the Middle Miocene. However, the reconstructions of Kürschner et al. (2008) based on leaf stomatal indices indicate much higher MMCO CO₂ levels between 300 and 600 ppmv. Reconstructions based on paleosol analysis indicate an even higher CO₂ concentration of 850 ppmv (Retallack, 2009).

Alternatively, the reconfiguration of interoceanic passages which significantly influences the ocean circulation may have contributed to the MMCO climate (Bice et al., 2000; Von der Heydt and Dijkstra, 2008). The Central American Seaway and Eastern Tethys Seaway were notably open during the Middle Miocene (Herold et al., 2008), leading to significantly different ocean circulation patterns (Von der Heydt and Dijkstra, 2006).

Geological processes such as the mountain uplift may also affect the atmospheric

Middle Miocene climate modelling experiments

A.-J. Henrot et al.

Title Page

Abstract

Introduction

Conclusions

References

Tables

Figures



Back

Close

Full Screen / Esc

Printer-friendly Version

Interactive Discussion



circulation and precipitation patterns (Gregory-Wodzicki, 2000; Harris, 2006). Although the positions of the continents were close to modern, most of the higher orogens got elevated during the Miocene, such as the Himalayas and the Tibetan Plateau (Currie et al., 2005; Harris, 2006), the Central Andes (Gregory-Wodzicki, 2000) as well as the Alps (Kuhlemann et al., 2006). Topography was therefore generally lower at the Middle Miocene than at present-day (Herold et al., 2008).

Finally it should also be noticed that the warm climate prevailing during the Middle Miocene lead to vegetation changes. Broadleaved evergreen forests appear to have extended as far north as 45° N in North America and 52° N in Europe (Utescher et al., 2000). Such a change in the vegetation cover may have led to significant impacts on climate (Dutton and Barron, 1997).

Up to now, very few climate model simulations have been performed for the Middle Miocene. Climate modelling sensitivity experiments have particularly focused on the sensitivity of the Miocene climate to various atmospheric CO₂ concentrations using atmospheric models (Tong et al., 2009; You et al., 2009). You et al. (2009) have also analysed the sensitivity of MMCO climate to varying ocean heat fluxes and compared the global temperature estimations to proxy data. Recently, Herold et al. (2009) have tested the impact of topography changes related to Andean and Tibetan Plateau on the MMCO climate.

Here, we carry out a Middle Miocene sensitivity study with the Earth system model Planet Simulator. We perform a series of simulation experiments, where we have assessed the effects of the absence of ice on the continents, the opening of the Central American and Eastern Tethys Seaways, the lowering of the topography on land, the effect of various atmospheric CO₂ concentrations and the vegetation feedback in response to the Middle Miocene simulated climate. We first describe our model setup and examine the response of surface climate (temperature, precipitation and low level winds) to the different forcings. Finally, we discuss the contribution of the factors on the Middle Miocene climate, focusing in particular on the impact of topography changes on the European climate and the contribution of vegetation cover changes.

Middle Miocene climate modelling experiments

A.-J. Henrot et al.

Title Page

Abstract

Introduction

Conclusions

References

Tables

Figures



Back

Close

Full Screen / Esc

Printer-friendly Version

Interactive Discussion



2 Model and experimental design

The Planet Simulator (Fraedrich et al., 2005a,b) is an Earth system Model of Intermediate Complexity (EMIC). It has been used in various paleoclimatic studies focusing on different past periods (Romanova et al., 2006; Henrot et al., 2009), notably the late Miocene (Micheels et al., 2009b), and has proven usefulness in the comparison to proxy data (Henrot et al., 2009; Micheels et al., 2009a). The central component of the Planet Simulator is PUMA-2, a spectral GCM with triangular truncation, based upon the Portable University Model of the Atmosphere PUMA (Fraedrich et al., 1998). PUMA-2 solves the moist primitive equations, representing the conservation of momentum, mass and energy, on σ coordinates in the vertical. It also includes boundary layer, precipitation, interactive clouds and radiation parametrizations. For the present study, we configured it to use a T42 truncation and ten vertical equally spaced σ levels. The model atmosphere is coupled to a 50 m deep mixed-layer ocean, a thermodynamic sea-ice and a land surface and soil model.

Sea surface temperatures are computed from the net atmospheric heat flux at the surface. The transport of heat by oceanic surface currents is represented by an additional distribution of heat sources and sinks that is prescribed within the mixed-layer and the sea-ice and that varies monthly and spatially. Their distributions for the preindustrial period and the Middle Miocene were determined from preindustrial and Miocene experiments respectively, where sea surface temperature and sea-ice distributions were obtained from simulations with an updated version of the Hamburg LSG circulation model (developed by Maier-Reimer et al., 1993) (Butzin et al., 2010). This procedure allows the model to respond with a larger sensitivity to boundary condition changes than with prescribed sea-surface temperatures.

The land surface and soil models calculate the surface temperatures from a linearized energy balance equation and predict soil moisture on the basis of a simple bucket model. The influence of vegetation is represented by background albedo, roughness length and rooting depth. Their annual distributions are prescribed, and albedo

Middle Miocene climate modelling experiments

A.-J. Henrot et al.

Title Page

Abstract

Introduction

Conclusions

References

Tables

Figures



Back

Close

Full Screen / Esc

Printer-friendly Version

Interactive Discussion



**Middle Miocene
climate modelling
experiments**A.-J. Henrot et al.

[Title Page](#)[Abstract](#)[Introduction](#)[Conclusions](#)[References](#)[Tables](#)[Figures](#)[Back](#)[Close](#)[Full Screen / Esc](#)[Printer-friendly Version](#)[Interactive Discussion](#)

may only change in grid-cells where snow is present. The distributions of surface albedo, roughness length and rooting depth were obtained from a preindustrial run and a Middle Miocene run of the dynamic vegetation model CARAIB (CARbon Assimilation In the Biosphere) (Otto et al., 2002; François et al., 2006; Laurent et al., 2008). CARAIB calculates the carbon fluxes between the atmosphere and the terrestrial biosphere and deduces the evolution of carbon pools, together with the relative abundances of a series of plant functional types. Its different modules respectively focus on the hydrological cycle, photosynthesis and stomatal regulation, carbon allocation and biomass growth, heterotrophic respiration and litter and soil carbon, and the distribution of the model plant types, as a function of productivity. Here we used a classification including 15 Plant Functional Types (PFTs), described in Utescher et al. (2007) and Galy et al. (2008). Model derived PFT assemblages can be translated into biomes to produce vegetation maps. The inputs of the model are meteorological variables, taken from meteorological databases or GCM simulation experiments.

2.1 Experimental setup

In this work we examine the potential contribution of several boundary condition forcings to the MMCO. Therefore we perform a series of four sensitivity experiments where we have assessed the effects of the absence of ice on the continents, the opening of the Central American and Eastern Tethys Seaways, the lowering of the topography on land and of various atmospheric CO₂ concentrations. Table 1 lists the changes in boundary conditions applied for the series of experiments. The control experiment (CTRL) does not consider any of the changes and corresponds to a preindustrial state. Furthermore, we perform an additional simulation experiment, MM4-veg, testing the effect of vegetation cover changes on climate (through surface albedo, roughness length and rooting depth, i.e. bucket size) in response to the Middle Miocene simulated climate.

According to Flower and Kennett (1994) who place the major growth of the East Antarctic Ice-Sheet around 14.8 to 12.9 Ma (i.e. later than the MMCO), and Pekar and DeConto (2006) suggesting that only a reduced East Antarctic Ice-Sheet was present

Middle Miocene climate modelling experiments

A.-J. Henrot et al.

Title Page

Abstract

Introduction

Conclusions

References

Tables

Figures

◀

▶

◀

▶

Back

Close

Full Screen / Esc

Printer-friendly Version

Interactive Discussion



during the Middle Miocene (17 to 16 Ma), we removed ice-sheets from Antarctica and Greenland in the whole series of Miocene experiments. This mainly affects the surface albedo on land as the model does not include a dynamic ice-sheet model. In the absence of ice-sheets in Greenland and Antarctica the surface albedo is set equal to the bare soil value (20%). The continental land-ice cover for the (preindustrial) control experiment has been derived from Peltier's ICE-5G (Peltier, 2004), considering that grid-cells covered by an ice fraction greater than 50% are completely covered by ice.

There is currently no global proxy-based SST reconstruction available for the MMCO that could be directly used with GCMs. Furthermore several biases towards notably colder temperatures have been detected in the oxygen isotope paleo SST estimates (Pearson et al., 2007). We therefore preferred to use as initial conditions over ocean gridpoints sea-surface temperature and sea-ice distributions derived from simulations of the updated Hamburg LSG circulation model, which includes a simple atmospheric energy balance model permitting that the LSG SSTs freely adjust to ocean circulation changes (Butzin et al., 2010). Butzin et al. (2010) performed several simulation experiments to assess the sensitivity of benthic carbon isotope records to various seaway configurations and sea-ice scenarios. In this work, we used as initial oceanic conditions for the Miocene simulation experiments the sea-surface temperature and sea-ice distributions from one LSG simulation featuring open Central American and Eastern Tethys Seaways, a fixed atmospheric CO₂ concentration of 282 ppmv and sea ice extent around 90% of the present-day value. Preindustrial LSG results were also used to derive the preindustrial sea-surface temperature and sea-ice distributions for the control run of our series. The LSG sea-surface temperature and sea-ice cover for the preindustrial and the Miocene are shown in Fig. 1. In the Miocene LSG simulation, the opening of the Central American Seaway freshens the upper part of North Atlantic while salinities increase in the other oceans. Changes in the Meridional Overturning Circulation (MOC) in the Atlantic Ocean also lead to a cooling of the upper North Atlantic and a warming in the South Atlantic. The Eastern Tethys Seaway weakly impacts on Indian Ocean heat transport.

**Middle Miocene
climate modelling
experiments**

A.-J. Henrot et al.

Title Page

Abstract

Introduction

Conclusions

References

Tables

Figures



Back

Close

Full Screen / Esc

Printer-friendly Version

Interactive Discussion



The oceanic heat flux distributions for the preindustrial and the Miocene were calculated from preliminary runs using prescribed LSG sea-surface temperatures and sea-ice distributions as well as LSG land-sea distribution, topography and CO₂ concentration respectively for the preindustrial and the Miocene. The flux corrections obtained are shown in Fig. 2. The distributions of Miocene ocean currents show a weakening of the surface heat transfer to the North Atlantic due to the opening of the Central American Seaway, but an increase of the heat transfer to the South Atlantic. However, despite the reorganization of heat transfer in the Atlantic Ocean, the distribution of the surface currents at the Miocene does not differ much from the preindustrial distribution.

The use of LSG sea-surface temperatures as initial oceanic conditions imposed us to stick to the land-sea distribution and corresponding topography prescribed in the LSG experiments (Butzin et al., 2010). The control experiment was therefore forced with the present-day LSG land-sea mask and topography, whereas the Miocene experiments were forced with the Miocene LSG land-sea mask which takes into account an open Central American Seaway and an open Eastern Tethys Seaway (see Fig. 3). However, the Miocene LSG simulations consider a present-day topography on land. It is thought that elevation on land was globally lower during the Miocene (Ruddiman, 1997; Harris, 2006; Gregory-Wodzicki, 2000). We therefore applied the algorithm described in Kutzbach et al. (1989) in order to reconstruct a topography approximatively at half-height of its modern elevation.

$$h = 400 + (h_0 - 400)/2 \quad \text{where } h_0 \geq 400 \text{ m}$$

That algorithm halves the elevation only above a base level of 400 m to approximate a geologic situation in which some continental relief was present prior to geologically recent uplift (Kutzbach et al., 1989). The present-day and Miocene land-sea mask and topography are shown on Fig. 3. A more precise study would have used the recent Middle Miocene paleotopographic reconstruction by Herold et al. (2008), geographically constrained at 15 Ma. Unfortunately, the LSG land-sea distribution is incompatible with the paleogeography of Herold et al. (2008), especially regarding ocean gateways, which are central to the present study. Nevertheless, our Miocene adapted topography

agrees fairly well with the reconstruction of Herold et al. (2008), taking into account the model resolution. The elevations of the North American, European and African reliefs are comparable to the ones reported in Herold et al. (2008). However, the maximum elevation of the Tibetan Plateau is limited to 3500 m in our reconstruction, whereas Herold et al. (2008) constrained it to 4700 m. On the contrary, the Andes are around 500 m higher in our Miocene topography. Nevertheless, the differences between both topography reconstructions remains within the paleoelevation data errors for the Tibetan Plateau (Currie et al., 2005; Wang et al., 2006) and the Andes (Gregory-Wodzicki, 2000).

The vegetation parameters have been derived from a preindustrial vegetation distribution calculated from an equilibrium run of CARAIB, forced with 280 ppmv of CO₂ and the climatology of New et al. (2002). All of the experiments have been forced with the preindustrial vegetation distribution except for the experiment MM4-veg. In experiment MM4-veg, the vegetation parameters have been replaced by their Middle Miocene distributions derived from a vegetation distribution produced by CARAIB. We used an equilibrium run of CARAIB forced with 500 ppmv of CO₂ in the atmosphere and the climate derived from the experiment MM4, which is the warmest and most humid of the series and in best agreement with proxy-based climate reconstructions (see Sect. 4). We calculated the anomalies of the GCM climatic fields between the Middle Miocene and the preindustrial, added to the climatology of New et al. (2002), as climatic inputs for the Middle Miocene simulation, following the approach described in Otto et al. (2002).

We also forced our simulations with various atmospheric CO₂ concentrations. The control experiment, as well as the first Miocene simulation experiments MM1 and MM2 used a preindustrial CO₂ level of 280 ppmv. In experiment MM3 the CO₂ concentration was set to 200 ppmv. 200 ppmv is within the range given by marine isotopic reconstructions suggesting low and constant CO₂ levels throughout the Miocene (Pagani et al., 1999; Henderiks and Pagani, 2008; Pearson and Palmer, 2000). For experiment MM4 we adopted a value of 500 ppmv to test the hypothesis of high CO₂ levels during the

Middle Miocene climate modelling experiments

A.-J. Henrot et al.

Title Page

Abstract

Introduction

Conclusions

References

Tables

Figures

◀

▶

◀

▶

Back

Close

Full Screen / Esc

Printer-friendly Version

Interactive Discussion



Miocene suggested by terrestrial proxies (Kürschner et al., 2008; Retallack, 2009). Finally, in the whole series of experiments, we applied a present-day orbital configuration and solar constant.

3 Middle Miocene simulations as compared to the preindustrial control run

3.1 Global and zonal average temperature and precipitation

The four Middle Miocene experiments generally produce global temperature and precipitation increases when compared to the control run (experiment CTRL) (see Table 2). Experiment MM1 shows a global temperature increase of $+0.6^{\circ}\text{C}$ that is mainly due to oceanic warming and Antarctic and Greenland warming in the absence of land-ice, whereas the temperatures and precipitation on other continents decrease. The reduction of the topography in experiment MM2 generates the weakest effect on global temperature but significantly increases precipitation, especially on the continents. The weak global impact of the topography reduction on temperature can be attributed to local and opposed effects. We even obtain a cooling over the oceans while the continents warm. The lowering of the atmospheric CO_2 concentration (experiment MM3) produces a global cooling together with a precipitation reduction. Effects are stronger in terms of magnitude on the oceans due to the sea-ice albedo feedback. The increase of the atmospheric CO_2 concentration to 500 ppmv (experiment MM4) has the strongest effect on temperature of the series. It warms the global climate by $+2.9^{\circ}\text{C}$. The higher CO_2 level also reinforces the increase of precipitation caused by the reduction of the topography, especially on the continents, producing the strongest effects of the four experiments on precipitation.

The zonal surface air temperature (SAT) and precipitation means are shown in Fig. 4. The zonal average temperature and precipitation anomalies (EXPERIMENT – CTRL) are also shown in Fig. 5 to allow a finer comparison. The zonal temperature averages do not indicate large differences from the control experiment at any latitude, except

Middle Miocene climate modelling experiments

A.-J. Henrot et al.

Title Page

Abstract

Introduction

Conclusions

References

Tables

Figures



Back

Close

Full Screen / Esc

Printer-friendly Version

Interactive Discussion



Middle Miocene climate modelling experiments

A.-J. Henrot et al.

Title Page

Abstract

Introduction

Conclusions

References

Tables

Figures

◀

▶

◀

▶

Back

Close

Full Screen / Esc

Printer-friendly Version

Interactive Discussion



at high latitudes of both hemispheres. The warming at high latitudes linked to an increase of precipitation is due to the absence of ice on land. Moreover the absence of ice on Antarctica and Greenland generates a positive albedo feedback that reinforces the initial warming of these regions. The reduction of the topography produces localized warming mostly in the Northern Hemisphere but decrease the temperature at latitudes higher than 60° N. The reduction of the topography also decreases precipitation around 30° N but strongly increases them especially in the tropics around the ITCZ. The reduction of atmospheric CO₂ reinforces the general cooling trend and decreases the precipitation at all latitudes as compared to the results of experiment MM2. However, it does not disrupt the zonal profiles of SAT and precipitation. The increase of atmospheric CO₂ in experiment MM4 further reinforces the warming at high latitudes, reducing again the latitudinal temperature gradient. This additional warming can be attributed to the melting of sea-ice in warmer conditions. The CO₂ induced warming also contributes to increase the precipitation rate at all latitudes. In general, we observe that the zonal profiles of the precipitation distribution and precipitation anomalies are not strongly modified from experiment MM1, even if the topography on land is reduced.

3.2 Regional responses of temperature and precipitation

3.2.1 Regional patterns in experiment MM1

Figure 6 shows the annual mean surface air temperature (SAT) and precipitation anomalies between experiment MM1 and the control run CTRL. The strongest changes in the surface air temperature in response to the modified sea surface temperatures and land-sea mask mainly concern the oceans and continents of the Northern Hemisphere, whereas the precipitation disruptions mostly occur in the tropics. However, the local effects on temperature and precipitation are rather contrasted and no clear global warming or cooling trend can be made out in experiment MM1.

Large increases of the surface air temperature occur over Greenland and especially Antarctica. They are due to a decrease of the surface albedo (more than 40 to 60%)

**Middle Miocene
climate modelling
experiments**

A.-J. Henrot et al.

Title Page

Abstract

Introduction

Conclusions

References

Tables

Figures



Back

Close

Full Screen / Esc

Printer-friendly Version

Interactive Discussion



over ice-free land points in experiment MM1. This albedo feedback mainly affects the summer of the hemisphere. In winter it can be overruled by the influence of surrounding colder oceanic air masses, which notably lead to a net cooling over Greenland in winter.

Significant changes in surface air temperature as well as in precipitation are observed especially over the oceans. These are a consequence of the sea surface temperature modification in response to ocean circulation changes in the Miocene LSG simulation. The reduction of the heat transfer to the North Atlantic leads to large decreases of SAT in that region. Colder and drier conditions are obtained in the Mexican Gulf but the strongest decrease of SAT of up to -6°C , occurs in the North Atlantic, along the south coast of Greenland. This region also experiences a large decrease of precipitation linked to the cooling of the air masses. The colder conditions over the North Atlantic induce continental temperature decreases together with precipitation increase, notably over northwestern Europe and Africa in winter. However, the colder and drier conditions in the Equatorial Atlantic induce an increase of SAT of more than 1°C linked to a decrease of precipitation of about -400 mm/yr over the northern part of South America and the east coast of North America.

In the Pacific Ocean, the opening of the Central American Seaway induces strong warming, reaching $+4^{\circ}\text{C}$ along the west coast of North America together with a precipitation increase. This brings warmer and more humid air masses from the West to the Center of North America and warmer air masses to the East after the passage of the high North American reliefs.

On the other hand, the opening of the Eastern Tethys Seaway influences the SAT in Central Asia and East Africa. A strong increase of SAT is observed over the Tethys Seaway and is mainly linked to the decrease of surface albedo produced by the change of land-sea mask. Precipitation is also strongly increased over the open seaway. As mentioned before, the opening of the Eastern Tethys Seaway weakly impacts on Indian Ocean heat transport. The western part of the Indian Ocean does not show any significant changes in SAT when compared to the CTRL experiment. The land points surrounding the open seaway experience colder conditions, except in the Indian

peninsula. The SAT decreases can be attributed to the more humid conditions that prevails in the presence of an open Tethys Seaway. However, since precipitation is strongly decreased in India during summer, the warming in this region can be linked to a reduced monsoon activity in presence of an open Eastern Tethys Seaway. Strong decreases of precipitation also occur in Indonesia and South-East China, suggesting a reduced monsoon activity in these regions too. Finally, the SAT cools by about -2°C in eastern Russia, extending the cooling trend over Europe to the east.

3.2.2 Regional patterns in experiments MM2

Figures 7 and 8, respectively, show the annual and seasonal surface air temperature and precipitation anomalies between experiments MM2 and CTRL. The summer and winter low-level winds (850 hPa) for experiment CTRL and MM2 are also shown in Fig. 9 to allow a more complete analysis of the topographic effects. Strong and localized warming occurs in the location of the present-day high reliefs that are directly affected by the largest topography reduction. Altitude reductions of more than 1000 m in some areas increases the annual mean SAT by more than $+10^{\circ}\text{C}$, e.g. in some parts of the Tibetan Plateau, the Andes, the Rockies, Greenland and Antarctica. In contrast to the continental warming, the SAT decreases over the oceans, especially in the Northern Hemisphere. The reduction of the topography also strongly disturbs the annual precipitation anomaly distribution on the continents. The anomalies show large differences when compared to the anomalies in experiment MM1. Northern and western Europe experience SAT decrease that extends to the east. The annual anomaly essentially reflects the colder conditions that affect Eurasia in summer, whereas warmer conditions prevail in winter. Precipitation also strongly increases over northern Europe especially in summer. Seasonal effects can be due to a more zonal atmospheric surface circulation in the presence of lower reliefs. Therefore stronger and more direct winds from the North Atlantic flow across Europe and penetrate deeper into the continent, bringing more humid and colder conditions in summer and more humid and warmer conditions in winter, weakening temperature and precipitation seasonal contrast over Europe.

Middle Miocene climate modelling experiments

A.-J. Henrot et al.

Title Page

Abstract

Introduction

Conclusions

References

Tables

Figures



Back

Close

Full Screen / Esc

Printer-friendly Version

Interactive Discussion



Middle Miocene climate modelling experiments

A.-J. Henrot et al.

Title Page

Abstract

Introduction

Conclusions

References

Tables

Figures

◀

▶

◀

▶

Back

Close

Full Screen / Esc

Printer-friendly Version

Interactive Discussion

This strong effect of the lower reliefs on the precipitation distribution in northern Europe is discussed in more detail in Sect. 3.2.3. Westerly winds coming from the North American continent instead of the Labrador Sea also flow over the North Atlantic, decreasing the activity of the Iceland low pressure cell. However, the southern part of Europe experiences an increase of SAT that is linked to the reduction of topography in the Alps and other reliefs, inducing local warming that dominates over the other effects. Furthermore, this warming can be reinforced in winter by a decrease of snowfall, resulting from the positive snow albedo feedback.

North America is affected by extended warming of more than +2°C that persists throughout the year. A precipitation increase in the North is induced by the direct contribution of humid air masses from the North Pacific especially in winter. In the absence of high reliefs, the winds flow directly to the west coast of North America and do not supply Alaska with humid air masses anymore. The isolation of the Alaska region leads to colder and drier conditions there in winter. The more zonal atmospheric surface circulation also contributes to isolate the Arctic Ocean that experiences strong winter cooling together with a precipitation decrease. In the center of North America, the lower Rockies also weaken the frontal zone activity in summer between air masses coming from the West and the East. This leads to a decrease of precipitation in summer that contributes to warm the region.

The decrease of the height of the Tibetan Plateau also produces large seasonal impacts. SAT increases for the whole year over China and eastern Russia, but decreases over India, Indonesia and Australia. As expected, a lower Tibetan Plateau contributes to weaken the Indian monsoon activity, which is characterized by a decrease of precipitation in summer. The summer precipitation also decrease in Indonesia and the eastern Equatorial Pacific, where the surface winds weaken. North-East China gets drier during the whole year, due to a strenghtening of the continental winds coming from the North-East in winter, but a decrease of the South-East winds in summer, which bring less humidity.

Middle Miocene climate modelling experiments

A.-J. Henrot et al.

Title Page

Abstract

Introduction

Conclusions

References

Tables

Figures



Back

Close

Full Screen / Esc

Printer-friendly Version

Interactive Discussion



Africa is affected by an increase of SAT that can be directly attributed to the topographic reduction in the North and the South-East. However, SAT decreases in West and Central Africa. This last effect comes together with a strong increase of precipitation, that can be attributed to the deeper penetration of westerly winds from the Atlantic together with a deeper penetration of north-easterly winds, which come from the moist region of the open Eastern Tethys Seaway. The northern part of South America also experiences a decrease of SAT together with an strong increase of precipitation.

3.2.3 Effects of the topography on precipitation in Europe

The lowering of the high reliefs causes a strong increase of precipitation together with a SAT decrease from northwestern to northeastern Europe. This is essentially a summer effect and is linked to a modification of the summer surface wind strength and direction. In order to determine the singlemost important topography change responsible for the precipitation disruption in Europe, we carried out several variants of experiment MM2, lowering separately and together the North American and European reliefs. We ran three additional sensitivity experiments, reducing the topography in Europe (between 15° W and 30° E and 25° N to 75° N) (experiment MM2-E), in North America (between 165° W and 60° W and 15° N to 75° N) (experiment MM2-A) and both together (experiment MM2-AE). We only lowered the North American and European reliefs for this series of tests. The other reliefs were hold at their respective present-day elevations. We also performed additional sensitivity experiments testing separately the effects of the lowering of the Tibetan Plateau, African reliefs and South American reliefs on the precipitation distribution in Europe. Effects on European precipitation and teleconnections found in these later experiments were rather weak, and we do not discuss those results any further here.

The disruption of summer precipitation and the summer winds at 850 hPa in absence of European reliefs are shown in Fig. 10. The lower reliefs in North Europe allow stronger westerly winds that come more directly from the Atlantic Ocean to penetrate deeper into the continent, bringing more humid and cold oceanic air masses to

**Middle Miocene
climate modelling
experiments**A.-J. Henrot et al.

[Title Page](#)[Abstract](#)[Introduction](#)[Conclusions](#)[References](#)[Tables](#)[Figures](#)[Back](#)[Close](#)[Full Screen / Esc](#)[Printer-friendly Version](#)[Interactive Discussion](#)

northern Europe. Nevertheless, the lowering of the North European reliefs alone is not sufficient to form the wet tongue that we obtained in experiment MM2. The lowering of the North American reliefs also produces stronger and more direct summer westerly winds in northwestern Europe, generating more precipitation in the region (see Fig. 11).

5 However, the presence of the North European reliefs stops the wetter air masses coming from the West, and does not allow the wet tongue obtained in experiment MM2 to form neither. Precipitation increases similar to those found in experiment MM2 are only obtained when the effects of European and North American topography changes are combined (Fig. 12). We conclude that the reduction of topography in North America
10 and Europe is necessary to produce the colder and wetter conditions that prevail in North Europe in experiment MM2. However, the wet tongue does not extend to the East as far as it does in experiment MM2. We can therefore attribute the increase of precipitation in North West Asia to the reduction of the topography in Asia.

3.2.4 Regional patterns in experiments MM3 and MM4

15 The surface air temperature and precipitation anomalies between experiments MM3 and CTRL and experiments MM4 and CTRL are shown in Fig. 13. The 80 ppmv lowering of the CO₂ concentration reduces the continental warming induced directly by the reduction of the topography, e.g. in eastern Africa and North America. The CO₂ decrease also reinforces the continental and oceanic cooling linked to the topogra-
20 phy induced disruptions, e.g. in northwestern Europe. Stronger cooling also occurs at high latitudes, especially over the Arctic Ocean, due to sea-ice feedback. However, the decrease of the CO₂ concentration does not disrupt the precipitation distribution when compared to experiment MM2. It slightly reinforces the precipitation decreases produced by the reduction of topography.

25 The increase of the atmospheric CO₂ concentration in experiment MM4 has a quasi global warming effect. The warming is more marked over the continents since the reduction of the topography already induced strong continental warming whereas it cooled the oceans. The higher CO₂ concentration therefore reinforces the SAT

Middle Miocene climate modelling experiments

A.-J. Henrot et al.

Title Page

Abstract

Introduction

Conclusions

References

Tables

Figures



Back

Close

Full Screen / Esc

Printer-friendly Version

Interactive Discussion



increases and weakens the SAT decreases produced by the reduction of the topography (experiment MM2). However, the effect of CO₂ can also more than counterbalance the effect of the topography on some regions. Northwestern Europe notably experiences significant increases of temperature in experiment MM4, whereas the reduced topography alone induced a cooling in that region (see Sect. 3.2.3). The higher CO₂ concentration also produces a strong warming at high latitudes and especially over the Arctic Ocean due to the melting of sea-ice, whereas the reduction of topography in experiment MM2 cooled the region. However, the higher CO₂ concentration does not disturb the precipitation distribution induced by the reduction of the topography in experiment MM2. The distributions of the precipitation anomalies are quite similar in experiments MM2 and MM4. The CO₂ effect reinforces the precipitation increases especially in the tropics. The topographic effects seem, however, to dominate the CO₂ effect, e.g., persistence of the wet tongue in northern Europe.

3.3 Focus on vegetation feedback

The warmer and more humid conditions prevailing in experiment MM4 could lead to significant vegetation cover modifications that could in turn affect the climate. Here, we analyse the results of experiment MM4-veg, taking into account the vegetation changes in response to the MM4 climate, in order to quantify the order of magnitude and the local impacts of vegetation changes on the MMCO climate.

The vegetation distribution obtained with CARAIB from the climate of experiment MM4 is shown in Fig. 14 and compared to the preindustrial natural vegetation distribution used in the rest of the experiments. Note that the vegetation maps do not show Antarctica, because the New et al. (2002) climatology does not include any data point in Antarctica. Globally, in response to the warmer and more humid climate in experiment MM4, the simulated Miocene vegetation distribution demonstrates an expansion of forest biomes at the expense of grasslands and desert. Tundra and temperate forest expand at high latitudes mainly at the expense of polar desert. Desertic and semi-desertic areas are strongly reduced and replaced by grasslands or warm

**Middle Miocene
climate modelling
experiments**A.-J. Henrot et al.

[Title Page](#)[Abstract](#)[Introduction](#)[Conclusions](#)[References](#)[Tables](#)[Figures](#)[Back](#)[Close](#)[Full Screen / Esc](#)[Printer-friendly Version](#)[Interactive Discussion](#)

and open woodlands, especially in Central Asia where desert completely disappears. Thermophilous types included in the subtropical forest biome expand particularly in South and Central Europe, due to the warmer and wetter conditions prevailing in the region. This results seems to be consistent with the reconstruction of Utescher et al. (2007), which suggests the presence of warm mixed and broadleaved evergreen forest in South and Central Europe. However, the drier conditions at the east coast of North America and in Southeastern China lead to the replacement of subtropical forest by warm and open woodlands.

The effect of vegetation changes on surface air temperature and precipitation is shown in Fig. 15. Only the anomalies between experiments MM4-veg and MM4 are shown in order to isolate the vegetation effects from the other forcings applied in experiment MM4. In comparison with experiment MM4 the vegetation changes produce an additional global warming of $+0.5^{\circ}\text{C}$ ($+0.4^{\circ}\text{C}$ on the oceans and $+0.6^{\circ}\text{C}$ on the continents) and an increase of precipitation of $+19\text{ mm/yr}$ ($+4\text{ mm/yr}$ on the oceans and $+58\text{ mm/yr}$ on the continents). The vegetation contribution is comparable in terms of magnitude but slightly lower than the local contributions of topography and high atmospheric CO_2 level. As described in Sect. 2, vegetation cover changes affect surface albedo and roughness length, but the albedo impact on surface temperature is dominant, because of its direct impact on the energy balance. However, the changes in rooting depth mainly affect the water cycle and therefore precipitation.

The vegetation cover changes produce a warming of 1 to 2°C essentially on the continents. Only the the Arctic Ocean experiences a warming of the same order due to the melting of sea-ice induced by the warming of the surrounding continental grid-points. Strong warming occurs around the Eastern Tethys Seaway. It is due to the decrease of surface albedo (not shown) produced by the replacement of desert and semi-desert by open woodland, which develops in the more humid conditions produced by the opening of the seaway. Central Asia also experiences a decrease of surface albedo linked to the replacement of desert by forest. SAT increases in South and Central Europe due to the development of subtropical forest with a lower albedo. However, SAT decrease

in the Center and South of North America as well as in Northeastern China. This effect is linked to the increase of surface albedo induced by the opening of the landscape in response to the reduction of precipitation in these regions. The precipitation are essentially affected by vegetation changes in the tropical regions. The development of forest around the Eastern Tethys Seaway increases the soil water content (not shown) leading to an increase of evaporation and precipitation. The same effect occurs in central Asia. The precipitation increase in Equatorial Africa is due to the expansion of the tropical forest which enhances the hydrological cycle. The precipitation decrease in the west coast of Europe is due to the replacement of temperate forest by open woodlands, which decreases the soil water content.

4 Discussion

In the series of sensitivity tests that we carried out, several experiments resulted in an increase of the global surface air temperature. The increase of the atmospheric CO₂ concentration to 500 ppmv in experiment MM4 produces the largest global warming of the series of four experiments, as compared to the warming produced by sea surface temperature changes (experiment MM1) or reduced topography (experiment MM2). A lower CO₂ concentration however cools the global climate. A higher CO₂ concentration seems therefore necessary to generate a warmer climate in the Middle Miocene. However the warming we obtained is much lower than suggested by proxy data (Mosbrugger et al., 2005; Zachos et al., 2001), with middle latitudes temperatures up to +6 °C higher than present (Flower and Kennett, 1994). Nevertheless, our results agree fairly well with the results of previous modelling studies focusing on the Middle Miocene climate. Tong et al. (2009) tested the sensitivity of the Middle Miocene climate to various concentrations of atmospheric CO₂ using the NCAR model (CAM v.3.1) and Community Land Model (CLM v.3.0) coupled to a slab ocean model. They obtained a global warming of +0.6 °C for an atmospheric CO₂ concentration of 355 ppmv and a global warming of +2.9 °C for an atmospheric CO₂ concentration of 700 ppmv

Middle Miocene climate modelling experiments

A.-J. Henrot et al.

Title Page

Abstract

Introduction

Conclusions

References

Tables

Figures



Back

Close

Full Screen / Esc

Printer-friendly Version

Interactive Discussion



**Middle Miocene
climate modelling
experiments**

A.-J. Henrot et al.

in comparison to a present-day control run with a reference CO₂ concentration equal to 379 ppmv. You et al. (2009) used the same model to test the effect of various CO₂ concentration together with several sea surface temperature gradients. They obtained temperature increases of +2.3 °C for an atmospheric CO₂ concentration of 350 ppmv and a high SST gradient and of +3.5 °C for CO₂ at 700 ppmv and a medium SST gradient. Micheels et al. (2009a) used the Planet Simulator to test the sensitivity of the Late Miocene climate to various CO₂ concentrations. They obtained similar warmings, between +2.3 °C for 280 ppmv and +3.7 °C for 460 ppmv in comparison to a preindustrial control run with a CO₂ concentration of 280 ppmv.

The model results consistently indicate that a higher than present-day CO₂ concentration is necessary to produce a warm Middle Miocene climate (You et al., 2009; Tong et al., 2009). In that sense, the model results support the terrestrial proxy reconstruction of CO₂ level suggesting higher atmospheric CO₂ concentrations at MMCO, between 300 and 850 (Kürschner et al., 2008; Retallack, 2009). Conversely modelling results do not support the low CO₂ concentration, between 140 and 300 ppmv, derived from marine isotopic records, that suggest a decoupling between CO₂ and temperature during the Middle Miocene (Henderiks and Pagani, 2008; Pearson and Palmer, 2000). Experiments using lower CO₂ concentrations generate colder climate than at present-day (experiment MM3 in this study or Tong et al., 2009; You et al., 2009). However, as recently emphasised by Diester-Haass et al. (2009), a high CO₂ level at the Middle Miocene would be difficult to reconcile with the high $\delta^{13}\text{C}$ values of benthic foraminifera, which suggest large deposition rates of organic carbon tending to reduce atmospheric CO₂ levels. Therefore we should interpret the model results with great care. We indeed do not take into account all the possible effects that could contribute to the Middle Miocene warm climate. We notably miss the feedback of climate on ocean circulation at Middle Miocene that could only be simulated with a fully coupled ocean-atmosphere model, since we used a slab ocean model as in previous studies (Tong et al., 2009; You et al., 2009). The opening of ocean gateways notably at low latitudes seems to have strongly contributed to modify the global ocean circulation in the

Title Page

Abstract

Introduction

Conclusions

References

Tables

Figures

◀

▶

◀

▶

Back

Close

Full Screen / Esc

Printer-friendly Version

Interactive Discussion



Cenozoic in comparison to present-day (Bice et al., 2000; Von der Heydt and Dijkstra, 2008). We also only tested the effect of various CO₂ concentrations on climate given the large uncertainty in CO₂ estimations. We did not take into account a change in the concentrations of other atmospheric greenhouse gases such as methane. The potential role of such feedbacks is well illustrated by the results of our simulation experiment MM4-veg, which takes into account the feedback on climate from changing vegetation cover compared to the first four simulation experiments of our series.

In our series experiment MM1 assesses the effect of the MMCO SST distribution, as simulated by the LSG model (Butzin et al., 2010) and the corresponding surface ocean heat flux on climate. These changes produce contrasted effects on surface air temperature and precipitation over the oceans that influence the climatic conditions on land. The reduction of the oceanic heat transfer to the North Atlantic due to the opening of the Central American Seaway brings colder conditions over the North Atlantic and northwestern Europe. This effect agrees with the majority of published modelling studies results indicating that the closure of the Central American Seaway was responsible for increased oceanic heat transport to the North Atlantic that brought warmer conditions and ultimately increased precipitation in the Northern Hemisphere (Lunt et al., 2008; Schneider and Schmittner, 2006). The decrease of precipitation in South Asia, linked to SST changes, indicates a weakening of the Asian monsoon. According to Tschuck et al. (2004), the weakening of the Asian monsoon can be linked to the increase of sea surface temperatures in the equatorial Indian ocean and western Pacific Ocean. Therefore, the warmer conditions induced in the Pacific by the opening of the Central American Seaway may be contributing to the reduction of the precipitation in some parts of Asia.

Experiment MM2 allows us to discuss the climatic effects of the reduced topography on land. It also represents a Middle Miocene state with a preindustrial CO₂ concentration of 280 ppmv, since experiment MM2 includes all of the Middle Miocene boundary conditions considered in this study. As already demonstrated by Kutzbach et al. (1989), the reduction of the topography allows a more zonal atmospheric circulation and the

Middle Miocene climate modelling experiments

A.-J. Henrot et al.

Title Page

Abstract

Introduction

Conclusions

References

Tables

Figures



Back

Close

Full Screen / Esc

Printer-friendly Version

Interactive Discussion



**Middle Miocene
climate modelling
experiments**

A.-J. Henrot et al.

Title Page

Abstract

Introduction

Conclusions

References

Tables

Figures

◀

▶

◀

▶

Back

Close

Full Screen / Esc

Printer-friendly Version

Interactive Discussion

westerly flow to continue over the lowered Plateaus at mid-latitudes, e.g. the Colorado Plateau, the Tibetan Plateau and European reliefs. Moreover, the reduced height of the Tibetan Plateau prevents the development of a monsoon-like circulation (Kutzbach et al., 1989; Harris, 2006) that induces a strong decrease of precipitation notably over India. Recently, Herold et al. (2009) focused on the effect of lowered Tibetan Plateau and Andes on the Middle Miocene climate using the NCAR model (CAM v.3.1) and Community Land Model (CLM v.3.0) coupled to a slab ocean model with fixed sea-surface temperatures. Herold et al. (2009) also obtained strong local warming and a significant disruption of the surface winds due to the reduction of elevation over the Tibetan Plateau. However, the prescription of fixed sea-surface temperature in their experiment precluded a response of the ocean and therefore of the Asian monsoon system. Nevertheless, they also pointed out that the lowering of the Tibetan Plateau leads to a cooling linked to snow depth increase in Central Eurasia. In experiment MM2, the reduction of the topography leads to slight warming in Eurasia. Therefore, we can attribute the Eurasian warming in our results to the local increase of temperature induced by the reduction of reliefs higher than 400 m in the region. Unfortunately, our setup does not allow us to isolate the influence on Eurasia of the Tibetan Plateau elevation change. The lowering of North American and European reliefs produces wetter and colder conditions over northwestern Europe that are in disagreement with proxy-based reconstructions of the European Middle Miocene climate (Mosbrugger et al., 2005). However, the reduction of the seasonal gradient and the warming in South and Central Europe agree well with several reconstructions of the Middle Miocene climate based on pollen analysis (Jimenez-Moreno and Suc, 2007) and mega- or microfloral records (Mosbrugger et al., 2005; Utescher et al., 2007). Moreover, the reconstruction of Utescher et al. (2007) and other reconstructions based on the analysis of small mammals (Van Dam, 2006) show evidence for the persistence of a European wet zone during the Miocene, in agreement with our results. Nevertheless, the maximum increases of precipitation are located further north in Europe where no proxy reconstruction is available.

**Middle Miocene
climate modelling
experiments**

A.-J. Henrot et al.

Title Page

Abstract

Introduction

Conclusions

References

Tables

Figures

◀

▶

◀

▶

Back

Close

Full Screen / Esc

Printer-friendly Version

Interactive Discussion

In the last two experiments we test the effect of various CO₂ concentrations on the middle Miocene climate. Consistently with the results of Tong et al. (2009), the continental warming we obtained with a higher CO₂ concentration exceeds the oceanic warming. Generally, the stronger continental warming can be explained by the additional warming on land produced by the reduction of topography. However, north-western Europe shows a slight increase of temperature, since the topography induced effect cooled the region. Both topography reduction and increased CO₂ concentration contribute to wetter and warmer conditions in Europe, in better agreement with the proxies reconstructions (Mosbrugger et al., 2005; Utescher et al., 2007). As in Tong et al. (2009), the increase of the CO₂ concentration warms the high latitudes reducing the latitudinal gradient and also increases the precipitation, especially over the Arctic Ocean. The increase of the CO₂ concentration also enhances the hydrological cycle in the tropics, according to Tong et al. (2009). Nevertheless the activity of the monsoon system is still reduced in experiment MM4. This confirms the dominant effect of topography on the Asian monsoon system as compared to the CO₂ contribution (Tong et al., 2009).

Experiment MM4-veg finally allows us to investigate the vegetation feedback on climate in response to a warm and humid climate for the MMCO. The simulated vegetation distribution forced with the climate of experiment MM4 mainly demonstrates a reduction of the desertic and sub-desertic areas in the benefit of grasslands and forests, as well as an expansion of warm forest types poleward of the subtropical zone. This fairly agrees with the Middle Miocene data-based vegetation reconstruction used as boundary condition in the study of Tong et al. (2009), despite the differences in plant types classifications. Our vegetation distribution also agrees over South and Central Europe with the reconstruction of Utescher et al. (2007), which suggests the presence of warm mixed and broadleaved evergreen forest in South and Central Europe. Consistently with the data from Jimenez-Moreno and Suc (2007), CARAIB also yields warm and open mixed forest in Southwestern Europe, whereas it leads to thermophilous and mesothermic elements in Central Europe. Such a change in the vegetation cover

contributes to maintain and even to increase the warm and humid conditions that prevailed in experiment MM4. Moreover, the vegetation feedback on climate is of the same order of magnitude than the topographic or CO₂ effects, confirming the importance of the vegetation contribution to the MMCO climate. Therefore, vegetation-climate interactions could provide a complementary, if not an alternative mechanism, to the large increase of CO₂ required by the model to produce the estimated warming at MMCO.

5 Conclusions

In this study, we examine the potential contribution of several boundary condition changes to the warm climate of the Middle Miocene and particularly the Middle Miocene Climatic Optimum (MMCO). We used the Planet Simulator, an Earth System model of intermediate complexity to investigate the contributions of the absence of ice on the continents, the opening of the Central American and Eastern Tethys Seaways, the lowering of the topography on land and the effect of various atmospheric CO₂ concentrations on the Middle Miocene climate. We also investigated the retroaction of vegetation on climate. Therefore, we prescribe vegetation cover changes derived from a MMCO vegetation distribution produced by the dynamic vegetation model CARAIB, forced with the climate of the warmest and most humid experiment of the series. The boundary condition changes generally produce global warming in the Middle Miocene which are consistent with previous Middle Miocene sensitivity experiments (Tong et al., 2009; You et al., 2009). However, the increases of temperature we obtained are lower than the ones supported by proxy data (Zachos et al., 2001; Bruch et al., 2007).

The increase of the atmospheric CO₂ concentration to 500 ppmv produces the largest global warming of the series and contributes to warm the climate at all latitudes, similar to Tong et al. (2009). Therefore, a higher than present day CO₂ concentration seems necessary to produce the warm climate of the MMCO. This results support the terrestrial proxy reconstruction suggesting higher atmospheric CO₂ concentrations at MMCO (Kürschner et al., 2008; Retallack, 2009), but do not support the

Middle Miocene climate modelling experiments

A.-J. Henrot et al.

Title Page

Abstract

Introduction

Conclusions

References

Tables

Figures



Back

Close

Full Screen / Esc

Printer-friendly Version

Interactive Discussion



decoupling between CO₂ and temperature during the Middle Miocene suggested by the marine isotopic CO₂ reconstructions (Henderiks and Pagani, 2008; Pearson and Palmer, 2000).

However, we didn't take into account all the possible mechanisms that could contribute to the Middle Miocene warm climate. Therefore, our results could not state high level of CO₂ as primary driver for the Middle Miocene Climatic Optimum. We notably could not take into account the complete ocean-atmosphere feedback loop that could be simulated with a fully coupled ocean-atmosphere model. We furthermore did not take into account a change in the concentrations of other atmospheric greenhouse gases such as methane. The vegetation feedback could also plays an important role in the warm MMCO climate, as demonstrated by the last experiment testing the vegetation cover change feedback. In response to warm and humid conditions, forest expands at the expense of desert and warm forest types develop poleward of the subtropical zone. Such a change in vegetation cover leads to stronger warming and increase of precipitation. This confirms the contribution of vegetation in the MMCO warm climate and emphasises the need for data-model comparison in order to estimate the reliability of climate model experiments and vegetation reconstructions.

The topographic and oceanic forcings applied here have lower impact on the global temperature than CO₂ forcing, due to many opposite local effects. However, they significantly affect the temperature and precipitation distributions and their local effects can overpass the CO₂ effect. The opening of the Central American Seaway mainly reduces the oceanic heat transfer to the North Atlantic bringing colder conditions over the North Atlantic and northwestern Europe whereas the western Pacific warms, leading to a weakening of the Asian monsoon activity according to Tschuck et al. (2004). The reduction of the topography on land induces local increases of surface temperature. The lower topography allows a more zonal atmospheric circulation and the westerly flow to continue over the lowered Plateaus at mid-latitudes. The reduced height of the Tibetan Plateau notably prevents the development of a monsoon-like circulation (Kutzbach et al., 1989; Harris, 2006). This effect persists even at higher CO₂ concentration, which

Middle Miocene climate modelling experiments

A.-J. Henrot et al.

Title Page

Abstract

Introduction

Conclusions

References

Tables

Figures

◀

▶

◀

▶

Back

Close

Full Screen / Esc

Printer-friendly Version

Interactive Discussion



enhances the hydrological cycle in the tropics, affirming the dominant role of topography on the Asian monsoon system. Our results also highlight the effect of the reduction of elevations of the North American and European reliefs, which strongly increases precipitation but decreases surface air temperature from northwestern to eastern Europe. The colder conditions obtained over northern Europe disagree with proxy reconstruction of the European Middle Miocene climate (Mosbrugger et al., 2005), but the reduction of the seasonal gradient and the wetter conditions agree well with several proxy-based reconstructions (Jimenez-Moreno and Suc, 2007; Utescher et al., 2007; Mosbrugger et al., 2005).

Acknowledgements. We acknowledge the efforts of the Planet Simulator team (especially Klaus Fraedrich, Edilbert Kirk and Frank Lunkeit) for making available their model as Open Source Software and for the sustained development and help. A.-J. Henrot is a Research Fellow and G. Munhoven a Research Associate with the Belgian Fund for Scientific Research (F.R.S.-FNRS). We acknowledge support for this research from F.R.S.-FNRS under research grant “Crédit aux chercheurs” 1.5.179.07 F. This work is a contribution to the Deutsche Forschungsgemeinschaft project “Understanding Cenozoic Climate Cooling (UCCC)” (FOR 1070).

References

- Bice, K. L., Scotese, C. R., Seidov, D., and Barron, E. J.: Quantifying the role of geographic changes in Cenozoic ocean heat transport using uncoupled atmosphere and ocean models, *Earth Planet. Sci. Lett.*, 161, 295–310, 2000. 491, 509
- Bruch, A. A., Uhl, D., and Mosbrugger, V.: Miocene climate in Europe. Patterns and evolution: A first synthesis of NECLIME, *Palaeogeogr., Palaeoclimatol., Palaeoecol.*, 253, 1–7, 2007. 491, 512
- Butzin, M., Lohmann, G., and Bickert, T.: Miocene ocean circulation inferred from marine carbon cycle modeling combined with benthic isotope records, *Paleoceanography*, in review, 2010. 493, 495, 496, 509
- Currie, B. S., Rowley, D. B., and Tabor, N. J.: Middle Miocene paleoaltimetry of Southern Tibet: implications for the role of mantle thickening and delamination in the Himalayan orogen, *Geology*, 33, 181–184, 2005. 492, 497

Middle Miocene climate modelling experiments

A.-J. Henrot et al.

Title Page

Abstract

Introduction

Conclusions

References

Tables

Figures

◀

▶

◀

▶

Back

Close

Full Screen / Esc

Printer-friendly Version

Interactive Discussion



**Middle Miocene
climate modelling
experiments**A.-J. Henrot et al.

[Title Page](#)[Abstract](#)[Introduction](#)[Conclusions](#)[References](#)[Tables](#)[Figures](#)[◀](#)[▶](#)[◀](#)[▶](#)[Back](#)[Close](#)[Full Screen / Esc](#)[Printer-friendly Version](#)[Interactive Discussion](#)

- Diester-Haass, L., Billups, K., Gröcke, D., François, L., Lefebvre, V., and Emeis, K.: Mid-Miocene paleoproductivity in the Atlantic Ocean and Implications for the Global Carbon Cycle, *Paleoceanography*, 24, PA1011, doi:10.1029/2008PA001605, 2009. 508
- 5 Dutton, J. F. and Barron, E. J.: Miocene to present vegetation changes: A possible piece of the Cenozoic puzzle, *Geology*, 25, 39–41, 1997. 492
- Flower, B. P. and Kennett, J. P.: The Middle Miocene climatic transition: East Antarctic ice sheet development, deep ocean circulation and global carbon cycling, *Palaeogeogr., Palaeoclimatol., Palaeoecol.*, 108, 537–555, 1994. 491, 494, 507
- 10 Fraedrich, K., Kirk, E., and Lunkeit, F.: PUMA Portable University Model of the Atmosphere, Tech. Rep. 16, Meteorologisches Institut, Universität Hamburg, Hamburg, <http://www.mad.zmaw.de/fileadmin/extern/documents/reports/ReportNo.16.pdf>, 1998. 493
- Fraedrich, K., Jansen, H., Kirk, E., Luksch, U., and Lunkeit, F.: The Planet Simulator: Towards a user friendly model, *Meteorol. Z.*, 14, 299–304, doi:10.1127/0941-2948/2005/0043, 2005a. 493
- 15 Fraedrich, K., Jansen, H., Kirk, E., and Lunkeit, F.: The Planet Simulator : Green planet and desert world, *Meteorol. Z.*, 14, 305–314, doi:10.1127/0941-2948/2005/0044, 2005b. 493
- François, L., Ghislain, M., Otto, D., and Micheels, A.: Late Miocene vegetation reconstruction with the CARAIB model, *Palaeogeogr., Palaeoclimatol., Palaeoecol.*, 238, 302–320, 2006. 494
- 20 Galy, V., François, L., France-Lanord, C., Faure, P., Kudrass, H., Palhol, F., and Singh, S. K.: C4 plants decline in the Himalayan basin since the Last Glacial Maximum, *Quat. Sci. Rev.*, 27, 1396–1409, 2008. 494
- Gregory-Wodzicki, K. M.: Uplift history of the Central and Northern Andes: A review, *Geol. Soc. Am. Bull.*, 112, 1091–1105, 2000. 492, 496, 497
- 25 Harris, N.: The elevation history of the Tibetan Plateau and its implication for the Asian monsoon, *Palaeogeogr., Palaeoclimatol., Palaeoecol.*, 241, 4–15, 2006. 492, 496, 510, 513
- Henderiks, J. and Pagani, M.: Coccolithophore cell size and the Paleogene decline in atmospheric CO₂, *Earth Planet. Sci. Lett.*, 269, 575–583, 2008. 497, 508, 513
- Henrot, A.-J., François, L., Brewer, S., and Munhoven, G.: Impacts of land surface properties and atmospheric CO₂ on the Last Glacial Maximum climate: a factor separation analysis, *Clim. Past*, 5, 183–202, 2009, <http://www.clim-past.net/5/183/2009/>. 493
- 30 Herold, N., Seton, M., Müller, R. D., You, Y., and Huber, M.: Middle Miocene tectonic bound-

**Middle Miocene
climate modelling
experiments**

A.-J. Henrot et al.

Title Page

Abstract

Introduction

Conclusions

References

Tables

Figures

◀

▶

◀

▶

Back

Close

Full Screen / Esc

Printer-friendly Version

Interactive Discussion



ary conditions for use in climate models, *Geochem. Geophys. Geosyst.*, 9(10), Q10009, doi:10.1029/2008GC002046, 2008. 491, 492, 496, 497

Herold, N., You, Y., Müller, R. D., and Seton, M.: Climate model sensitivity to change in Miocene paleotopography, *Australian J. Earth Sci.*, 56, 1049–1059, 2009. 492, 510

5 Jimenez-Moreno, G. and Suc, J.-P.: Middle Miocene latitudinal climatic gradient in Western Europe: Evidence from pollen records, *Palaeogeogr., Palaeoclimatol., Palaeoecol.*, 253, 208–225, 2007. 510, 511, 514

Kuhlemann, J., Dunkl, I., Brügel, A., Spiegel, C., and Frisch, W.: From source terrains of the Eastern Alps to the Molasse Basin: Detrital record of non-steady-state exhumation, *Tectonophysics*, 413, 301–316, 2006. 492

10 Kürschner, W. M., Kvacek, Z., and Dilcher, D. L.: The impact of Miocene atmospheric carbon dioxide fluctuations on climate and the evolution of terrestrial ecosystems, *PNAS*, 105, 449–453, 2008. 491, 498, 508, 512

Kutzbach, J. E., Ruddiman, W. F., and Prell, W. L.: Sensitivity of Climate to late Cenozoic Uplift in Southern Asia and the American West: Numerical Experiments, *J. Geophys. Res.*, 94, 393–407, 1989. 496, 509, 510, 513

15 Laurent, J.-M., François, L., Bar-Hen, A., Bel, L., and Cheddadi, R.: European Bioclimatic Affinity Groups: data-model comparisons, *Global Planet. Change*, 61, 28–40, 2008. 494

Lunt, D. J., Valdes, P. J., Haywood, A., and Rutt, I. C.: Closure of the Panama Seaway during the Pliocene: implications for climate and Northern Hemisphere glaciation, *Clim. Dynam.*, 30, 1–18, 2008. 509

20 Maier-Reimer, E., Mikolajewicz, U., and Hasselmann, K.: Mean Circulation of the Hamburg LSG OGCM and Its Sensitivity to the Thermohaline Surface Forcing, *J. Phys. Oceanog.*, 23, 731–757, 1993. 493

25 Micheels, A., Bruch, A., and Mosbrugger, V.: Miocene climate modelling sensitivity experiments for different CO₂ concentrations, *Palaeontologia Electronica*, 12(2), 5A, 2009a. 493, 508

Micheels, A., Eronen, J., and Mosbrugger, V.: The Late Miocene climate response to a modern Sahara desert, *Global Planet. Change*, 67, 193–204, 2009b. 493

Mosbrugger, V., Utescher, T., and Dilcher, D. L.: Cenozoic continental climatic evolution of Central Europe, *PNAS*, 102, 14964–14969, 2005. 491, 507, 510, 511, 514

30 New, M., Lister, D., Hulme, M., and Makin, I.: A high-resolution data set of surface climate over global land areas, *Clim. Res.*, 21, 1–25, 2002. 497, 505

Otto, D., Rasse, D., Kaplan, J., Warnant, P., and François, L.: Biospheric carbon stocks recon-

**Middle Miocene
climate modelling
experiments**A.-J. Henrot et al.

structed at the Last Glacial Maximum : comparison between general circulation models using prescribed and computed sea surface temperatures, *Global Planet. Change*, 33, 117–138, 2002. 494, 497

Pagani, M., Arthur, M. A., and Freeman, K. H.: Miocene evolution of atmospheric carbon dioxide, *Paleoceanography*, 14, 273–292, 1999. 491, 497

Pearson, P. N. and Palmer, M. R.: Atmospheric carbon dioxide concentrations over the past 60 million years, *Nature*, 406, 695–699, 2000. 491, 497, 508, 513

Pearson, P. N., van Dongen, B. E., Nicholas, C. J., Pancost, R. D., Schouten, S., Singano, J. M., and Wade, B. S.: Stable warm tropical climate through the Eocene Epoch, *Geology*, 35, 211–214, 2007. 495

Pekar, S. F. and DeConto, R. M.: High-resolution ice-volume estimates for the early Miocene: Evidence for a dynamic ice sheet in Antarctica, *Palaeogeogr., Palaeoclimatol., Palaeoecol.*, 231, 101–109, 2006. 494

Peltier, W. R.: Global glacial isostasy and the surface of the ice-age Earth : the ICE-5G (VM2) Model and GRACE, *Annu. Rev. Earth Planet. Sci.*, 32, 49–111, 2004. 495

Retallack, G. J.: Refining a pedogenic-carbonate CO₂ paleobarometer to quantify a middle Miocene greenhouse spike, *Palaeogeogr., Palaeoclimatol., Palaeoecol.*, 281, 57–65, 2009. 491, 498, 508, 512

Romanova, V., Lohmann, G., and Grosfeld, K.: Effect of land albedo, CO₂, orography, and oceanic heat transport on extreme climates, *Clim. Past*, 2, 31–42, 2006, <http://www.clim-past.net/2/31/2006/>. 493

Ruddiman, W. F. (Ed.): *Tectonic Uplift and Climate Change*, Plenum Press, New York, NY, 1997. 496

Schneider, B. and Schmittner, A.: Simulating the impact of the Panamanian seaway closure on ocean circulation, marine productivity and nutrient cycling, *Earth Planet. Sci. Lett.*, 246, 367–380, 2006. 509

Shellito, C. J., Sloan, L. C., and Huber, M.: Climate model sensitivity to atmospheric CO₂ levels in the Early-Middle Paleogene, *Palaeogeogr., Palaeoclimatol., Palaeoecol.*, 193, 113–123, 2003. 491

Tong, J. A., You, Y., Müller, R. D., and Seton, M.: Climate model sensitivity to atmospheric CO₂ concentrations for the middle Miocene, *Global Planet. Change*, 67, 129–140, 2009. 492, 507, 508, 511, 512

Tschuck, P., Chauvin, F., Dong, B., and Arpe, K.: Impact of sea-surface temperature anomalies

[Title Page](#)[Abstract](#)[Introduction](#)[Conclusions](#)[References](#)[Tables](#)[Figures](#)[◀](#)[▶](#)[◀](#)[▶](#)[Back](#)[Close](#)[Full Screen / Esc](#)[Printer-friendly Version](#)[Interactive Discussion](#)

**Middle Miocene
climate modelling
experiments**A.-J. Henrot et al.

- in the Equatorial Indian Ocean and Western Pacific on the Asian summer monsoon in three general circulation models, *Int. J. Climatol.*, 24, 181–191, 2004. 509, 513
- Utescher, T., Mosbrugger, V., and Ashraf, A.: Terrestrial climate evolution in Northwest Germany over the last 25 million years, *Palaeogeogr., Palaeoclimatol., Palaeoecol.*, 15, 430–449, 2000. 492
- 5 Utescher, T., Erdei, B., François, L., and Mosbrugger, V.: Tree diversity in the Miocene forests of Western Eurasia, *Palaeogeogr., Palaeoclimatol., Palaeoecol.*, 253, 226–250, 2007. 494, 506, 510, 511, 514
- Van Dam, J. A.: Geographic and temporal patterns in the late Neogene (12–3 Ma) aridification of Europe. The use of small mammals as paleoprecipitation proxies, *Palaeogeogr., Palaeoclimatol., Palaeoecol.*, 238, 190–218, 2006. 510
- 10 Von der Heydt, A. and Dijkstra, H. A.: Effect of ocean gateways on the global ocean circulation in the late Oligocene and early Miocene, *Paleoceanography*, 21, PA1011, doi:10.1029/2005PA001149, 2006. 491
- 15 Von der Heydt, A. and Dijkstra, H. A.: The effect of ocean gateways on ocean circulation patterns in the Cenozoic, *Global Planet. Change*, 62, 132–146, 2008. 491, 509
- Wang, Y., Deng, T., and Biasatti, D.: Ancient diets indicate significant uplift of southern Tibet after ca. 7 Ma, *Geology*, 34, 309–312, 2006. 497
- You, Y., Huber, M., Müller, R. D., Poulsen, C. J., and Ribbe, J.: Simulation of the Middle Miocene Climate Optimum, *Geophys. Res. Lett.*, 36, L04702, doi:10.1029/2008GL036571, 2009. 492, 508, 512
- 20 Zachos, J., Pagani, M., Sloan, L., Thomas, E., and Billups, K.: Trends, rhythms and aberrations in global climate 65 Ma to present, *Science*, 292, 686–693, 2001. 491, 507, 512

[Title Page](#)[Abstract](#)[Introduction](#)[Conclusions](#)[References](#)[Tables](#)[Figures](#)[◀](#)[▶](#)[◀](#)[▶](#)[Back](#)[Close](#)[Full Screen / Esc](#)[Printer-friendly Version](#)[Interactive Discussion](#)

Middle Miocene climate modelling experiments

A.-J. Henrot et al.

Table 1. Description of the 5 simulation experiments. *P* refers to preindustrial conditions and *M* refers to Miocene conditions. Each one of the four columns corresponds to each of the four modified boundary conditions: ocean heat transfer, ice-sheet cover, atmospheric CO₂ and topography.

Simulation	Ocean	Ice	CO ₂	Topo	
CTRL	<i>P</i>	<i>P</i>	280	<i>P</i>	
MM1	<i>M</i>	<i>M</i>	280	<i>P</i>	
MM2	<i>M</i>	<i>M</i>	280	<i>M</i>	
MM3	<i>M</i>	<i>M</i>	200	<i>M</i>	
MM4	<i>M</i>	<i>M</i>	500	<i>M</i>	
MM4-veg	<i>M</i>	<i>M</i>	500	<i>M</i>	+MMCO veg.

Title Page

Abstract

Introduction

Conclusions

References

Tables

Figures

◀

▶

◀

▶

Back

Close

Full Screen / Esc

Printer-friendly Version

Interactive Discussion



Middle Miocene climate modelling experiments

A.-J. Henrot et al.

Table 2. Global, continental and oceanic annual mean near-surface temperature T_{2m} (°C) and precipitation (mm/yr) anomalies for the four Middle Miocene simulation experiments. The continental mean excludes the contribution from Antarctica since strong warming can be attributed due to the absence of ice that is not representative of the other effects on the continents. All results reported here are global means over the last 20 years of 50-year simulations, allowing 30 years for the model to equilibrate. The CTRL absolute values are shown for comparison.

	T_{2m} (°C)			Prc (mm/yr)		
	Global	Ocean	Continent	Global	Ocean	Continent
CTRL	12.3	15.3	11.6	1022	1138	803
Anomalies (EXPERIMENT-CTRL)						
MM1	+0.6	+0.5	-0.2	-5	+6	-38
MM2	+0.3	-0.5	+0.8	+20	+8	+38
MM3	-1.5	-2.1	-1	-14	-36	+28
MM4	+2.9	+2	+3.7	+73	+70	+85

[Title Page](#)
[Abstract](#)
[Introduction](#)
[Conclusions](#)
[References](#)
[Tables](#)
[Figures](#)
[Back](#)
[Close](#)
[Full Screen / Esc](#)
[Printer-friendly Version](#)
[Interactive Discussion](#)


Middle Miocene climate modelling experiments

A.-J. Henrot et al.

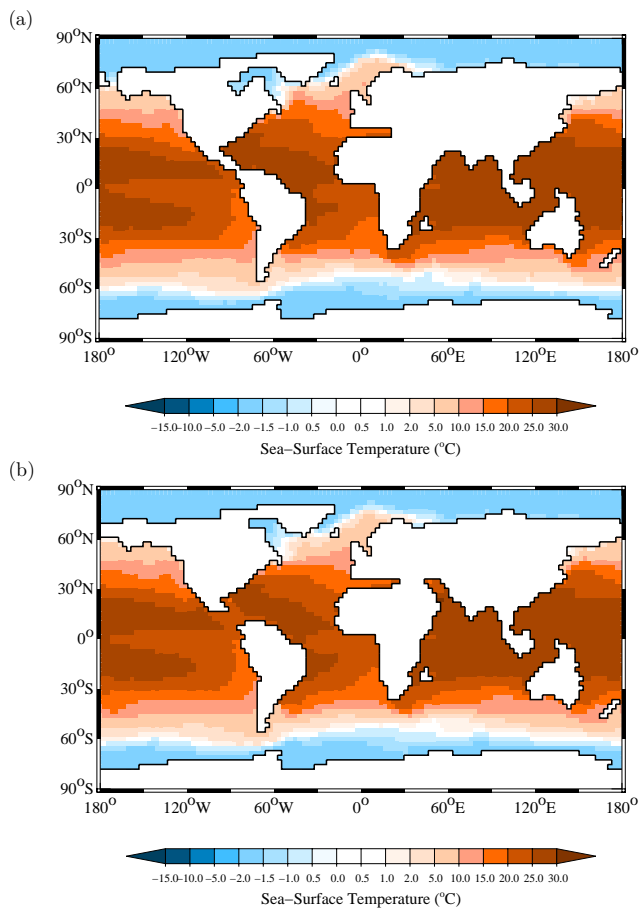


Fig. 1. Sea-surface temperatures for **(a)** the CTRL experiment and **(b)** the Miocene experiments. Sea-surface temperatures below -1.5°C indicate the presence of sea-ice on the corresponding pixel.

[Title Page](#)[Abstract](#)[Introduction](#)[Conclusions](#)[References](#)[Tables](#)[Figures](#)[◀](#)[▶](#)[◀](#)[▶](#)[Back](#)[Close](#)[Full Screen / Esc](#)[Printer-friendly Version](#)[Interactive Discussion](#)

Middle Miocene
climate modelling
experiments

A.-J. Henrot et al.

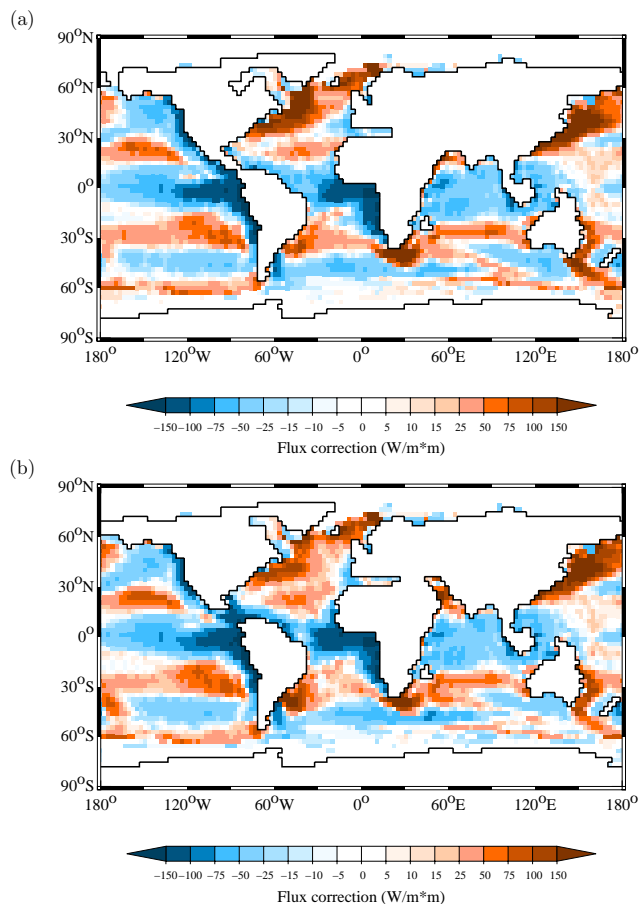


Fig. 2. Oceanic surface heat transfer for **(a)** the CTRL configuration and **(b)** the Miocene configuration. Positive values indicate a net transfer of heat from the ocean to the atmosphere.

[Title Page](#)[Abstract](#)[Introduction](#)[Conclusions](#)[References](#)[Tables](#)[Figures](#)[◀](#)[▶](#)[◀](#)[▶](#)[Back](#)[Close](#)[Full Screen / Esc](#)[Printer-friendly Version](#)[Interactive Discussion](#)

**Middle Miocene
climate modelling
experiments**

A.-J. Henrot et al.

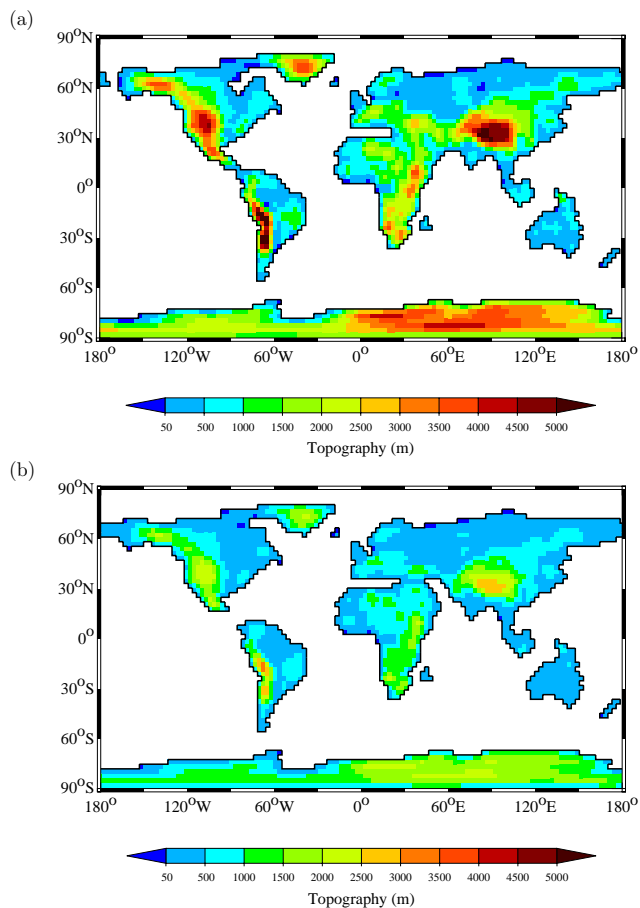


Fig. 3. Land-sea mask and topography on land for **(a)** the CTRL configuration and **(b)** the Miocene configuration.

[Title Page](#)[Abstract](#)[Introduction](#)[Conclusions](#)[References](#)[Tables](#)[Figures](#)[◀](#)[▶](#)[◀](#)[▶](#)[Back](#)[Close](#)[Full Screen / Esc](#)[Printer-friendly Version](#)[Interactive Discussion](#)

Middle Miocene climate modelling experiments

A.-J. Henrot et al.

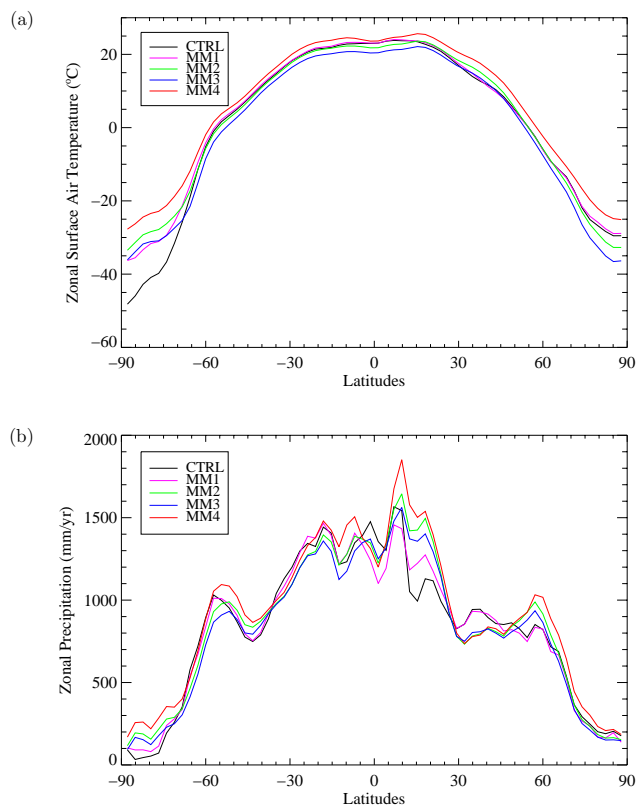


Fig. 4. Zonal average **(a)** surface air temperature (°C) and **(b)** precipitation (mm/yr) for the complete series of simulation experiments.

[Title Page](#)[Abstract](#)[Introduction](#)[Conclusions](#)[References](#)[Tables](#)[Figures](#)[◀](#)[▶](#)[◀](#)[▶](#)[Back](#)[Close](#)[Full Screen / Esc](#)[Printer-friendly Version](#)[Interactive Discussion](#)

**Middle Miocene
climate modelling
experiments**

A.-J. Henrot et al.

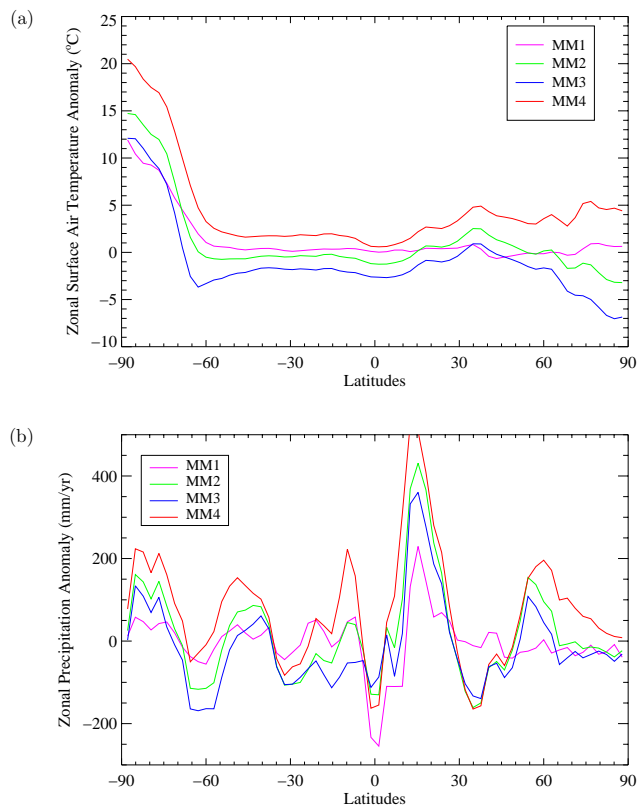


Fig. 5. Zonal average **(a)** surface air temperature anomalies (°C) and **(b)** precipitation anomalies (mm/yr) for the series of Middle Miocene simulation experiments.

[Title Page](#)[Abstract](#)[Introduction](#)[Conclusions](#)[References](#)[Tables](#)[Figures](#)[◀](#)[▶](#)[◀](#)[▶](#)[Back](#)[Close](#)[Full Screen / Esc](#)[Printer-friendly Version](#)[Interactive Discussion](#)

**Middle Miocene
climate modelling
experiments**

A.-J. Henrot et al.

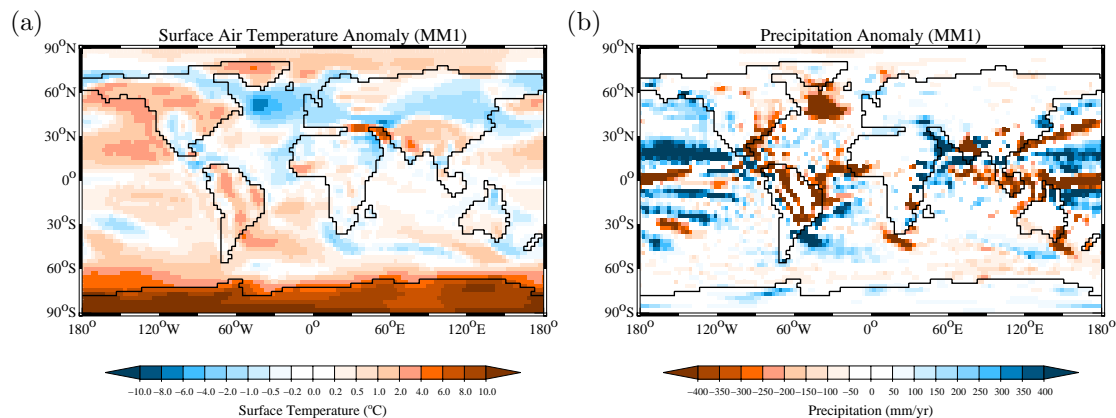
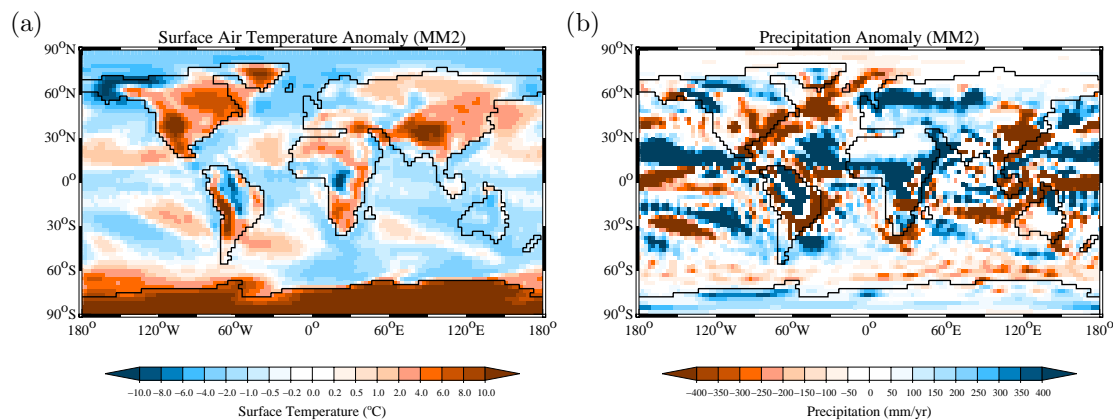


Fig. 6. (a) Annual surface temperature and (b) precipitation anomalies (EXPERIMENT-minus-CTRL) for experiment MM1. Only the precipitation anomalies greater than one standard deviation for the long-term annual mean over the last 20 simulation years are shown.

[Title Page](#)[Abstract](#)[Introduction](#)[Conclusions](#)[References](#)[Tables](#)[Figures](#)[⏪](#)[⏩](#)[◀](#)[▶](#)[Back](#)[Close](#)[Full Screen / Esc](#)[Printer-friendly Version](#)[Interactive Discussion](#)

**Middle Miocene
climate modelling
experiments**

A.-J. Henrot et al.

**Fig. 7.** Same as Fig. 6 for experiment MM2.[Title Page](#)[Abstract](#)[Introduction](#)[Conclusions](#)[References](#)[Tables](#)[Figures](#)[⏪](#)[⏩](#)[◀](#)[▶](#)[Back](#)[Close](#)[Full Screen / Esc](#)[Printer-friendly Version](#)[Interactive Discussion](#)

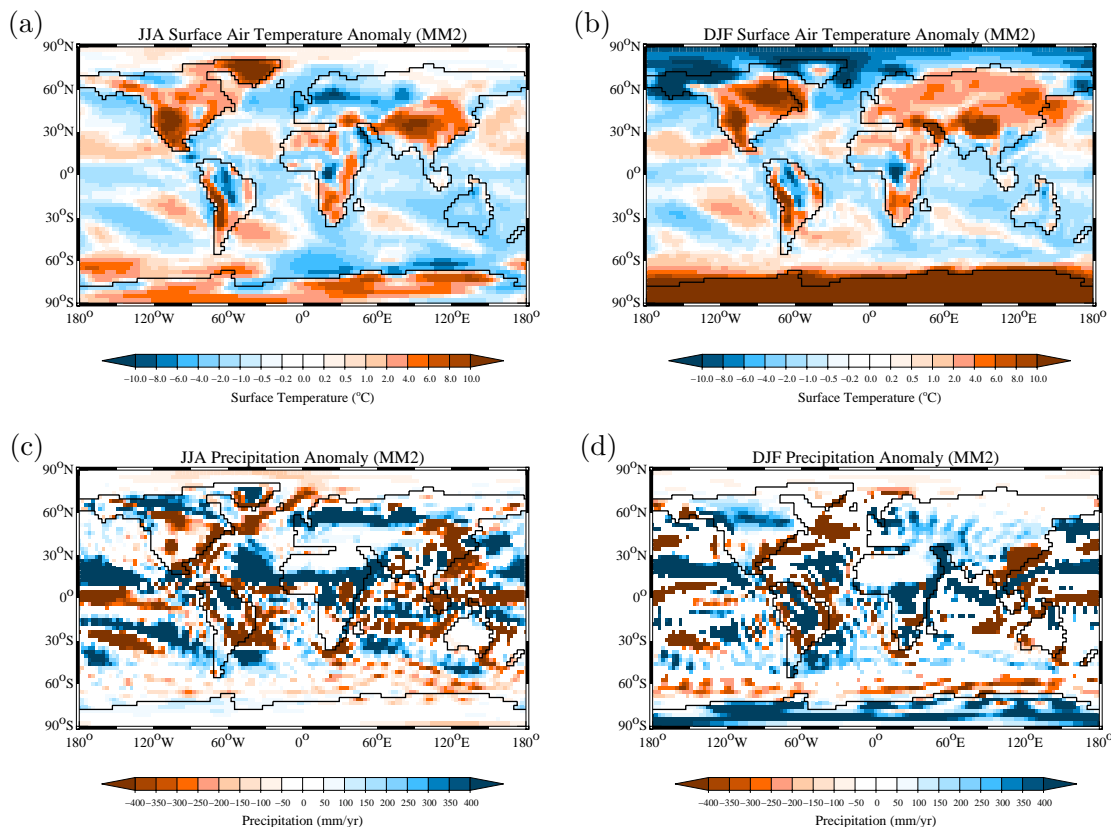


Fig. 8. Surface air temperature anomalies in (a) Northern Hemisphere summer (JJA) and (b) Northern Hemisphere winter (DJF) for experiment MM2. Precipitation anomalies in (c) Northern Hemisphere summer (JJA) and (d) Northern Hemisphere winter (DJF) for experiment MM2.

[Title Page](#)[Abstract](#)[Introduction](#)[Conclusions](#)[References](#)[Tables](#)[Figures](#)[◀](#)[▶](#)[◀](#)[▶](#)[Back](#)[Close](#)[Full Screen / Esc](#)[Printer-friendly Version](#)[Interactive Discussion](#)

Middle Miocene
climate modelling
experiments

A.-J. Henrot et al.

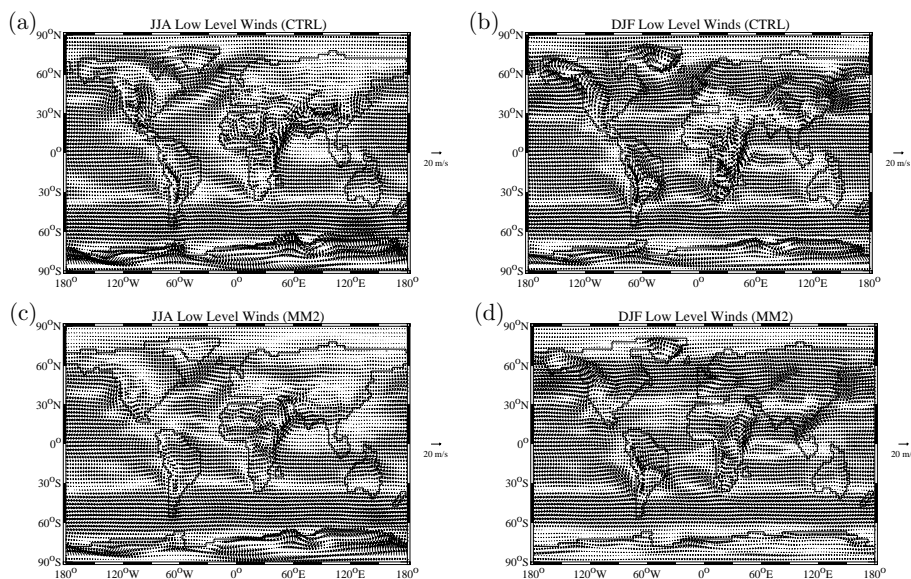


Fig. 9. CTRL low-level winds (850 hPa) in **(a)** Northern Hemisphere summer and **(b)** Northern Hemisphere winter. MM2 low-level winds (850 hPa) in **(c)** Northern Hemisphere summer and **(d)** Northern Hemisphere winter.

[Title Page](#)[Abstract](#)[Introduction](#)[Conclusions](#)[References](#)[Tables](#)[Figures](#)[◀](#)[▶](#)[◀](#)[▶](#)[Back](#)[Close](#)[Full Screen / Esc](#)[Printer-friendly Version](#)[Interactive Discussion](#)

Middle Miocene
climate modelling
experiments

A.-J. Henrot et al.

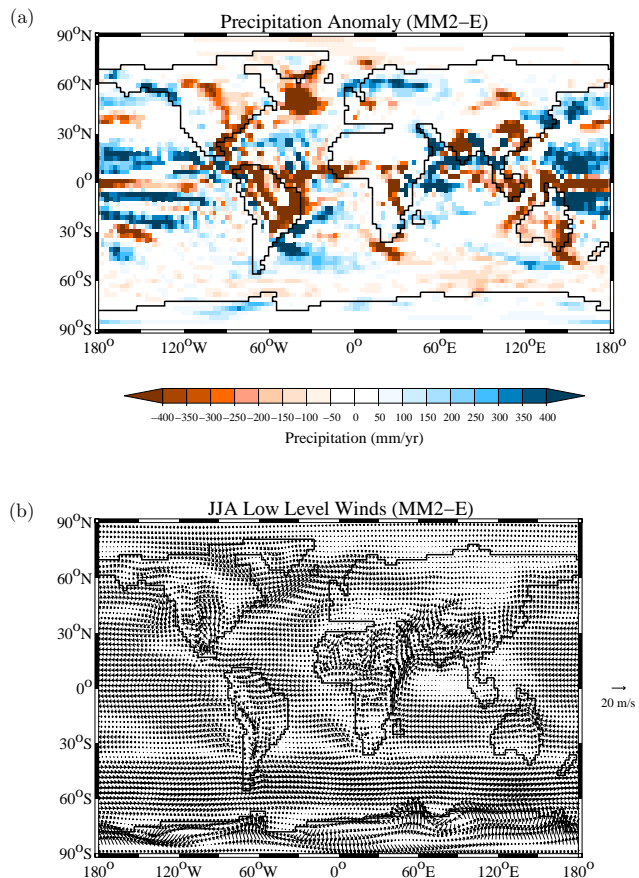


Fig. 10. (a) Annual precipitation anomalies and (b) Northern Hemisphere summer low-level winds (850 hPa) for experiment MM2-E.

[Title Page](#)[Abstract](#)[Introduction](#)[Conclusions](#)[References](#)[Tables](#)[Figures](#)[◀](#)[▶](#)[◀](#)[▶](#)[Back](#)[Close](#)[Full Screen / Esc](#)[Printer-friendly Version](#)[Interactive Discussion](#)

Middle Miocene
climate modelling
experiments

A.-J. Henrot et al.

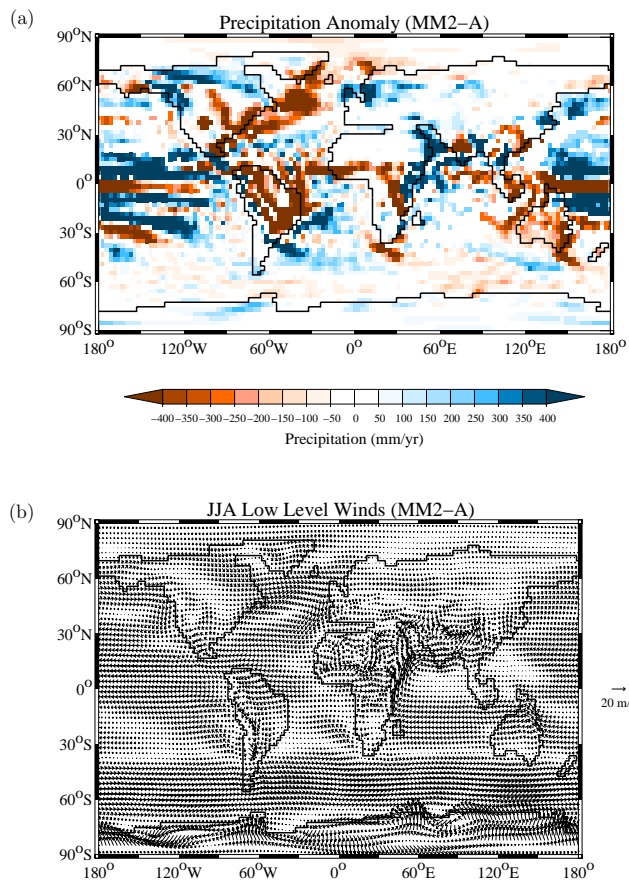
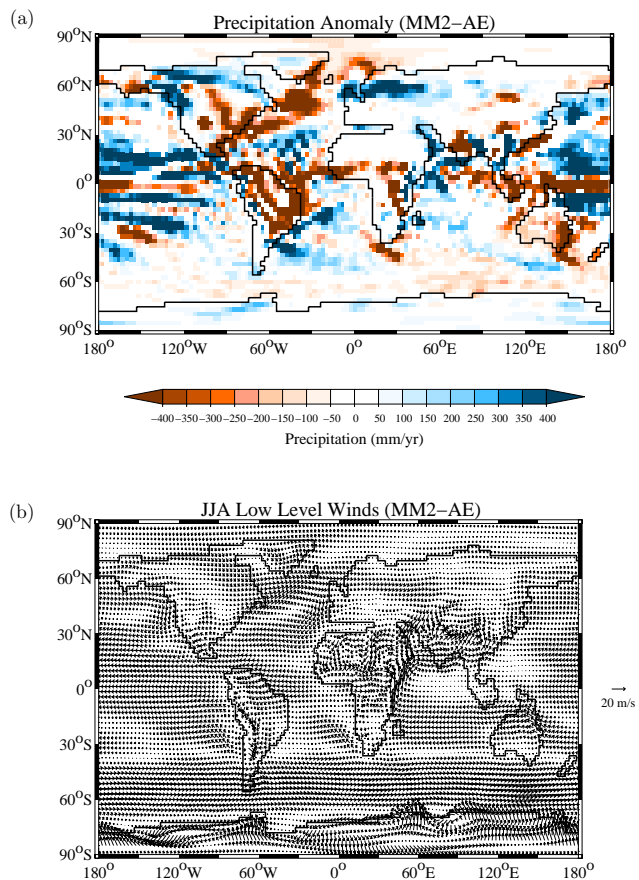


Fig. 11. Same as Fig. 10 for experiment MM2-A.

[Title Page](#)[Abstract](#)[Introduction](#)[Conclusions](#)[References](#)[Tables](#)[Figures](#)[◀](#)[▶](#)[◀](#)[▶](#)[Back](#)[Close](#)[Full Screen / Esc](#)[Printer-friendly Version](#)[Interactive Discussion](#)

**Middle Miocene
climate modelling
experiments**

A.-J. Henrot et al.

**Fig. 12.** Same as Fig. 10 for experiment MM2-AE.[Title Page](#)[Abstract](#)[Introduction](#)[Conclusions](#)[References](#)[Tables](#)[Figures](#)[◀](#)[▶](#)[◀](#)[▶](#)[Back](#)[Close](#)[Full Screen / Esc](#)[Printer-friendly Version](#)[Interactive Discussion](#)

Middle Miocene
climate modelling
experiments

A.-J. Henrot et al.

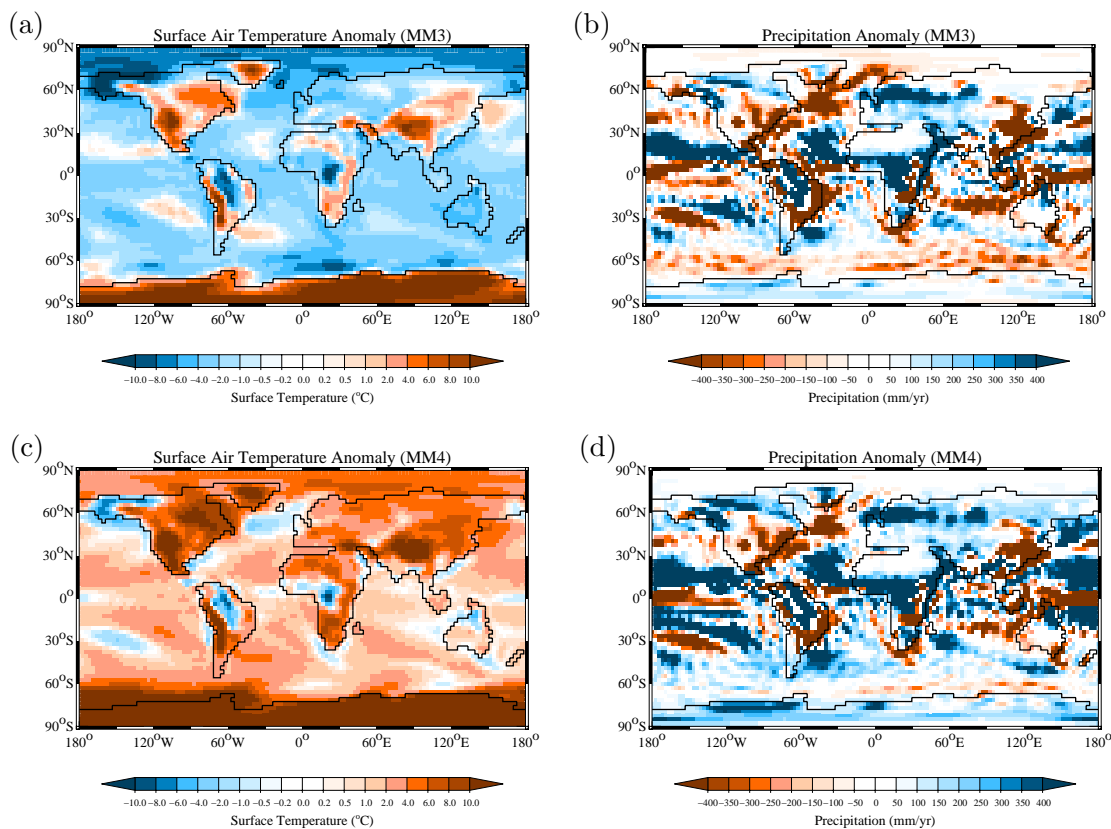


Fig. 13. (a) Annual surface temperature and (b) precipitation anomalies for experiment MM3. (c) Annual surface temperature and (d) precipitation anomalies for experiment MM4.

[Title Page](#)[Abstract](#)[Introduction](#)[Conclusions](#)[References](#)[Tables](#)[Figures](#)[◀](#)[▶](#)[◀](#)[▶](#)[Back](#)[Close](#)[Full Screen / Esc](#)[Printer-friendly Version](#)[Interactive Discussion](#)

Middle Miocene climate modelling experiments

A.-J. Henrot et al.

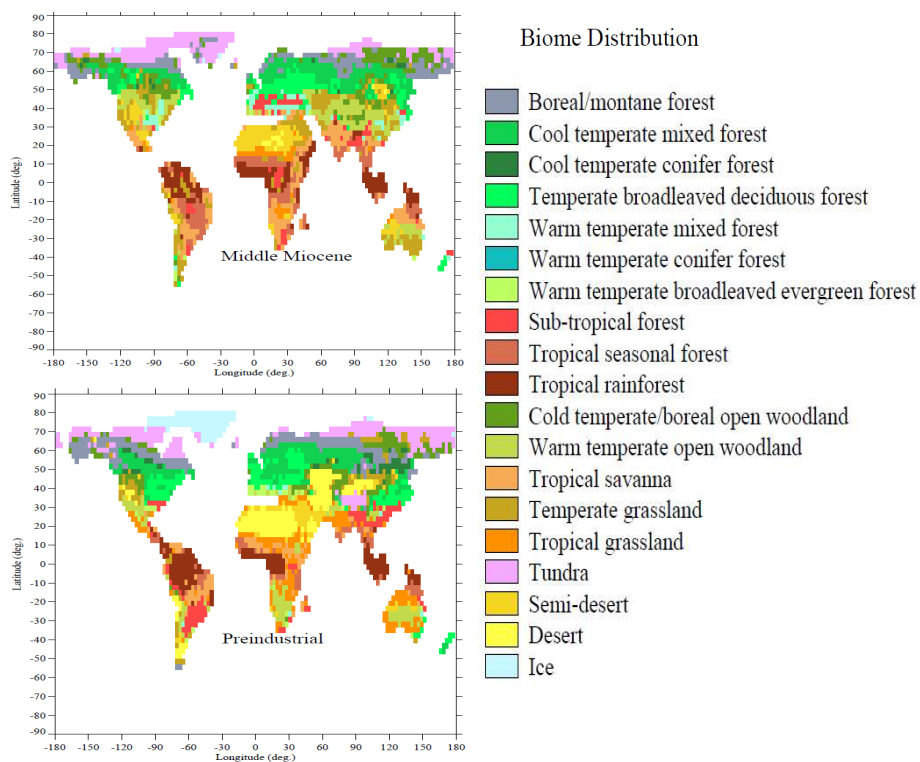


Fig. 14. Biome distributions from CARAIB preindustrial and MMCO equilibrium runs.

Title Page

Abstract

Introduction

Conclusions

References

Tables

Figures

◀

▶

◀

▶

Back

Close

Full Screen / Esc

Printer-friendly Version

Interactive Discussion



Middle Miocene climate modelling experiments

A.-J. Henrot et al.

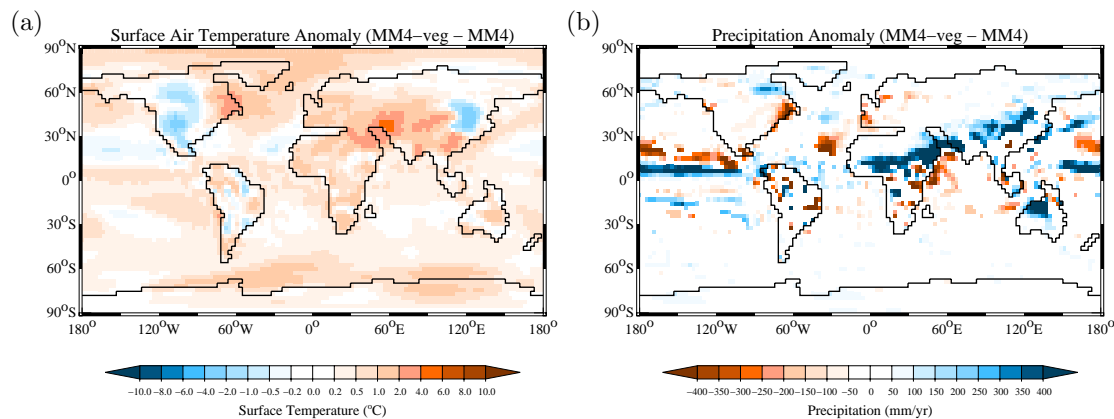


Fig. 15. (a) Annual surface temperature and (b) precipitation anomalies between experiment MM4-veg and MM4.

Title Page

Abstract

Introduction

Conclusions

References

Tables

Figures

◀

▶

◀

▶

Back

Close

Full Screen / Esc

Printer-friendly Version

Interactive Discussion

